Automated Backbone NMR Resonance Assignment of Large Proteins Using Redundant Linking from a Single Simultaneous Acquisition

Jan Stanek, Tobias Schubeis, Piotr Paluch, Peter Güntert, Loren B Andreas, Guido Pintacuda

Automated backbone NMR resonance assignment of large proteins using redundant linking from a single simultaneous acquisition

Jan Stanek,[#,‖,‡] Tobias Schubeis,[#,‡] Piotr Paluch,[‖] Peter Güntert,[&,§,=] Loren B Andreas,[#,⊥] and Guido Pintacuda[#,*]

[#]Centre de RMN à Très Hauts Champs, FRE (FRE 2034 CNRS, UCB Lyon 1, ENS Lyon), Université de Lyon, 5 rue de la Doua, 69100 Villeurbanne, France; [‖]Faculty of Chemistry, University of Warsaw, 02089 Warsaw, Poland; [⊥]Max Planck Institute for Biophysical Chemistry, Am Fassberg 11, D-37077 Göttingen, Germany, [&]Physical Chemistry, Eidgenössische Technische Hochschule Zurich, Zurich, Switzerland; [§]Center for Biomolecular Magnetic Resonance, Institute of Biophysical Chemistry, Goethe University Frankfurt, Frankfurt, Germany; [=]Department of Chemistry, Tokyo Metropolitan University, Hachioji, Japan

Supporting Information Placeholder

ABSTRACT: Thanks to magic-angle spinning (MAS) probes with frequencies of 60–100 kHz, the benefit of high sensitivity ^{1}H detection can now be broadly realized in biomolecular solid-state NMR for the analysis of microcrystalline, sedimented, or lipid-embedded preparations. Nonetheless, performing the assignment of all resonances remains a rate-limiting step in protein structural studies, and even the latest optimized protocols fail to perform this step when the protein size exceeds ~20 kDa. Here we leverage the benefits of fast (100 kHz) MAS and high (800 MHz) magnetic fields to design an approach that lifts this limitation. Through the creation, conservation and acquisition of independent magnetization pathways within a single triple-resonance MAS NMR experiment, a single self-consistent dataset can be acquired, providing enhanced sensitivity, reduced vulnerability to machine or sample instabilities, and highly redundant linking that supports fully-automated peak picking and resonance assignment. The method, dubbed RAVASSA (Redundant Assignment Via A Single Simultaneous Acquisition), is demonstrated with the assignment of the largest protein to date in the solid state, the 42.5 kDa maltose binding protein, using a single fully protonated microcrystalline sample and one week of spectrometer time.

INTRODUCTION

The proton is inherently the most sensitive nuclear spin since it has the highest gyromagnetic ratio among all stable isotopes. This is recognized in solution NMR spectroscopy, where standard acquisition schemes are centered around amide protons for protein resonance assignment and structure determination. For solid-state NMR, following years of pioneering developments,[2-5] the benefit of high sensitivity ^{1}H detection can now be broadly realized thanks to magic-angle spinning (MAS) probes with frequencies of 60–100 kHz[6-7] and beyond.[8] With these advances in instrumentation, high-resolution "fingerprint" correlation spectra can now be obtained for deuterated[9-10] and fully protonated proteins[11-12] and RNA[13] within minutes using a sub-milligram sample quantity. This has led to the development of a palette of triple-resonance experiments for accelerating the sequential assignment[1,14-17] and expanding the repertoire of proteins for which nearly complete resonance assignment can be obtained. Currently, however, the complexity of spectra in solids permits the analysis of microcrystalline, sedimented or lipid-embedded preparations of small proteins, and only few examples above 250 amino acid residues (aa) were reported, for which either deuteration[18-21] and/or a combination of differently labeled samples[12,22-24] was required.

A potential solution to overcome this size barrier is provided by the study of fully protonated proteins at 100 kHz MAS and above, with the design of complementary approaches based on the detection of narrow α-proton resonances.[25-26] However, the acquisition of such an expanded dataset also approximately doubles the spectrometer time required, which makes the entire acquisition vulnerable to machine or sample instabilities,[27] and increases severely the complexity of the data analysis. Deviations in peak position exceeding the linewidth are not unusual in these approaches, in particular if multiple samples are analyzed. While these deviations can sometimes be recognized by expert manual analysis, they can be catastrophic for automated approaches which rely on strict resonance matching thresholds.[28] With a manual approach, assignment of thousands of resonances is cumbersome and time consuming, commonly demanding years of data analysis. We show in the following that these issues can be addressed by automated analysis of a single self-consistent dataset composed of six simultaneously acquired ^{1}H-detected three-dimensional (3D) spectra employing MAS at frequencies exceeding 100 kHz. The method, hereafter dubbed redundant assignment via a single simultaneous acquisition (RAVASSA), enhances sensitivity, with a 2–3-fold reduction in experimental time, and results in spectra that support fully-automated peak picking and resonance assignment. We demonstrate its efficiency with the 371 aa maltose binding protein (MBP), using a single fully-protonated sample (< 1 mg of uniformly ^{13}C,^{15}N-labelled material).

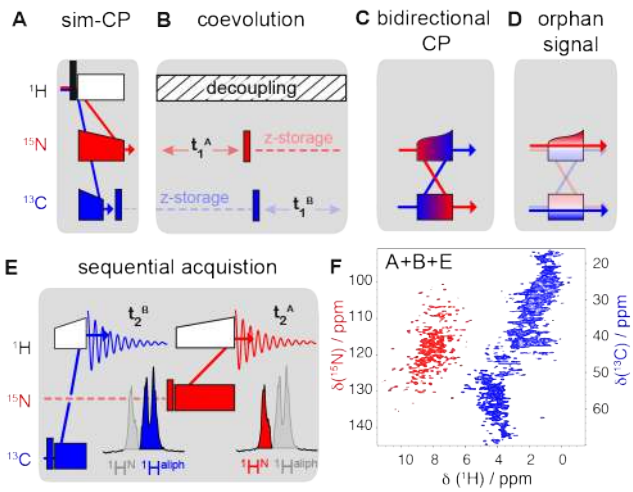

Figure 1. Scheme of radiofrequency building blocks for multiple pathway coherence transfers: (A) simultaneous cross-polarization of amide ^{15}N and ^{13}Cα spins from spatially proximal protons; (B) unconstrained co-evolution of ^{15}N and ^{13}C chemical shifts; (C) bidirectional ^{15}N–^{13}C CP without and (D) with recovery of orphan coherence; (E) a single scan sequential acquisition of α and amide ^{1}H signal following respective CPs from ^{13}Cα and ^{15}N. (F) Simultaneous dipolar-based ^{13}C,^{15}N-HSQC spectrum of maltose binding protein (see SI for a detailed RF scheme of this experiment).

RESULTS

Figure 1 depicts the key building blocks needed to implement RAVASSA, by creating, conserving and recording independent magnetization pathways within a single triple-resonance MAS NMR experiment: (A) simultaneous cross-polarization (SIM-CP) from ^{1}H to both ^{15}N and ^{13}C;[29-30] (B) co-evolution (time-sharing) of indirect ^{15}N and ^{13}C chemical shifts;[31] (C) bidirectional cross-polarization allowing simultaneous polarization transfer from ^{13}C to ^{15}N and vice-versa;[29] (D) recovery of orphan terms left over due to incomplete CP transfers;[32-33] and (E) separated acquisition of ^{1}Hα and ^{1}H^{N} signals, one occurring immediately after the other.[33] In panel (F), we show the simplest case of a co-acquired CP-^{13}C,^{15}N-HSQC[31,33] spectrum of MBP which takes advantage of blocks A, B and E. The amide and aliphatic 2D correlations were acquired simultaneously in 1 hour, as compared to 2 h for recording two separate spectra, on a 800 MHz spectrometer at 107 kHz MAS. Samples with 100% abundance of protons, which recently became available to proton-detected NMR analysis with ≥100 kHz MAS, are central to the performance of SIM-CP, since they contain independent reservoirs of ^{1}H magnetization for ^{1}H-^{15}N and ^{1}H-^{13}Cα pathways as demonstrated both experimentally and by quantum-mechanical calculations in Fig S1-S3. Note that, while our main focus here is on the backbone nuclei, simultaneous polarization in fully protonated proteins can also be exploited to generate correlations of side-chain spins, e.g. through-space contacts using broadband ^{1}H,^{1}H RFDR-techniques.[31] Concerning the mode of detection (Fig 1E), deferring the acquisition of ^{1}H^{N} signal comes at virtually no cost due to very slow relaxation of the ^{15}N *z*-polarization in solids (T_1 of the order of seconds).[29] Additionally, simpler radiofrequency (RF) conditions are used for separate "back" CP, and the cross-talk between pathways (^{15}N→^{1}Hα and ^{13}Cα→^{1}H^{N} transfers) is avoided. Also, ^{1}Hα and ^{1}H^{N} signals, with partially overlapping chemical shift ranges, are cleanly separated.

These design principles are used to construct the more complex pulse sequences discussed below. Figure 2 shows the pulse sequence for an implementation of RAVASSA based around a direct amide-to-amide transfer experiment (NNH).[15-16] A comparison of panels (A) and (B) shows the additional transfer blocks used to record a total of eight unique transfer pathways. The NNH scheme contains five coherence transfers between consecutive nuclei along the protein backbone and therefore contains multiple opportunities for the incorporation of the building blocks described above (see SI for detailed description of the pulse sequences). Simultaneous CP, coevolution and bidirectional CP naturally lead to acquisition of an analogous experiment for Hα-detected inter-residue Cα–Cα correlation (CCH) together with NNH. By retaining orphan spin operators (Fig1D) left after the ^{13}C–^{15}N CP, four additional spectra (and 2-fold redundant resonance linking, as described below) can be co-acquired, namely the intra- and inter-residue N–Cα–Hα and Cα–N–H^{N} correlations. Overall, a total of six useful pathways can be observed.

Figure 3 shows the resulting eight co-acquired spectra, together with representative data on MBP. A proper separation of data sets requires only a doubling of a spectral window in dimension ω_1, and one additional phase-cycle to discriminate pairs of pathways, without any impact on sensitivity. A trivial linear combination of data is used to extract the spectra arranged as shown in Figure 3A. Our implementation makes no compromise on resolution in any dimension, due to the possibility to extend periods of low power proton decoupling during each indirect evolution (see SI). Unconstrained chemical shift evolution times for ^{15}N and ^{13}C nuclei are indeed essential for the resolution of spectra for proteins as large as MBP. The experiment was performed in less than 5 days (instead of more than 16 days necessary with a regular acquisition) and showed excellent sensitivity, resolution and high information content, as demonstrated with heteronuclear (ω_1-ω_2) projections of component spectra in Figure 3B. Together, the four-fold redundant sequential linking of the resulting datasets provide highly fault tolerant data for backbone resonance assignment (Figure 3C). It consists of all combinations: ^{1}H^{N}–detected spectra with sequential correlations through (1) ^{13}Cα or (2) ^{15}N chemical shifts, and, symmetrically, ^{1}Hα-detected spectra correlated by (3) ^{15}N or (4) ^{13}Cα frequencies. Representative strips from six spectra are shown in Figure 3D. Completeness of the spectra is characterized by automatic identification of 275 to 309 cross-peaks out of a maximum 349 to 371 expected in particular spectra (1770 in total). Peaks were automatically identified using the routine embedded in the spectral analysis software CCPN,[34] and inevitably contained a certain fraction (approximately 15%) of noise peaks.

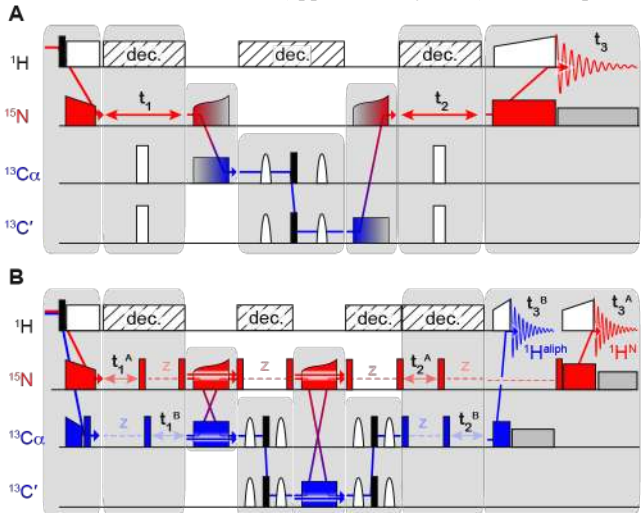

Figure 2. Simplified time diagram of RF irradiation for (A) conventional amide-to-amide proton transfer experiment (NNH)[15] and (B) its expansion using simultaneous excitation, coevolution and bidirectional CP transfers (RAVASSA).

The redundancy of information and consistency of chemical shifts in four assignment connectivities makes it perfectly amenable to automation and robust in the presence of spurious peaks.

For assignment automation, we turned to the exceptionally flexible automated resonance assignment algorithm FLYA[35] that has been applied to $^{13}C/^{15}N$-detected solid state data[36] and very large methyl-labeled proteins.[37] The algorithm accommodated unusual Hα–detected correlations with straightforward extensions of the FLYA library (provided in SI). Given the discontinuities in sequential linking due to 21 proline residues (6% of the sequence) or otherwise missing correlations, we expanded our data set by intraresidue (but not interresidue) correlations of either amide and α-protons to $^{13}C\beta$ shifts (namely (H)(CA)CB(CA)NH[38] and (H)(CA)CBCAH[25] spectra), which provide reliable information on a specific residue type and thus greatly help to locate fragments within the protein sequence. As demonstrated in Figure 4, small deviations of chemical shifts (approximately 0.1 and 0.3 ppm for ^{1}H and $^{13}C/^{15}N$ shifts) and high redundancy of information allowed to overcome critical ambiguity of resonance matching, typically encountered in large proteins, leading to approximately 82% complete assignment. This is in contrast to the previous state of the art based on the $^{1}H^{N}$-detection and matching of ^{13}C chemical shifts[1] (*black* curve in Figure 4), which was used to assign a suite of smaller proteins, but fails to assign more than 40% of MBP resonances regardless of matching tolerances. The lower limit for chemical shift tolerances is imposed by experimental linewidths and sensitivity, and for many important classes of samples (e.g., for integral membrane or fibrillar proteins) larger linewidths are typically found than observed for MBP. It is apparent from Figure 4 that the inherent ambiguity of the large protein MBP is beyond the capability for the five $^{1}H^{N}$-detected spectra, while the new approach leads to robust assignment. This is particularly apparent for higher tolerance values that correspond to the case of increased linewidths found for many important biological samples.

To further investigate the key component of RAVASSA, we restricted our data set by independently recording joint intra- and interresidue N–Cα–Hα and Cα–N–H^{N} correlations (pulse schemes provided in SI). This data also benefits from improved chemical shift consistency inherent for simultaneously acquired spectra, thus the limiting tolerances (lower limit) are identical to RAVASSA. In the case of MBP the extent of assignment is almost as good, however, the restricted data set breaks down rapidly with increasing matching tolerance (*blue* curve in Figure 4). It is therefore clear that the higher robustness of RAVASSA with respect to large linewidths stems from the NNH and CCH correlations. Interestingly, these correlations alone are clearly too ambiguous to yield a complete assignment in an automatic way (*cyan* curve in Figure 4). In FLYA, the four pathways support each other in resolving assignment ambiguities, with a significant cooperative effect (see supplementary Figure S12 for statistics on how often peaks from the different pathways are assigned for each residue). A relatively wide range of matching tolerances which provide reasonably complete automatic assignment (0.2–0.6 ppm for heteronuclei) not only simplifies the use of RAVASSA for samples different than studied here, but also suggests its power for

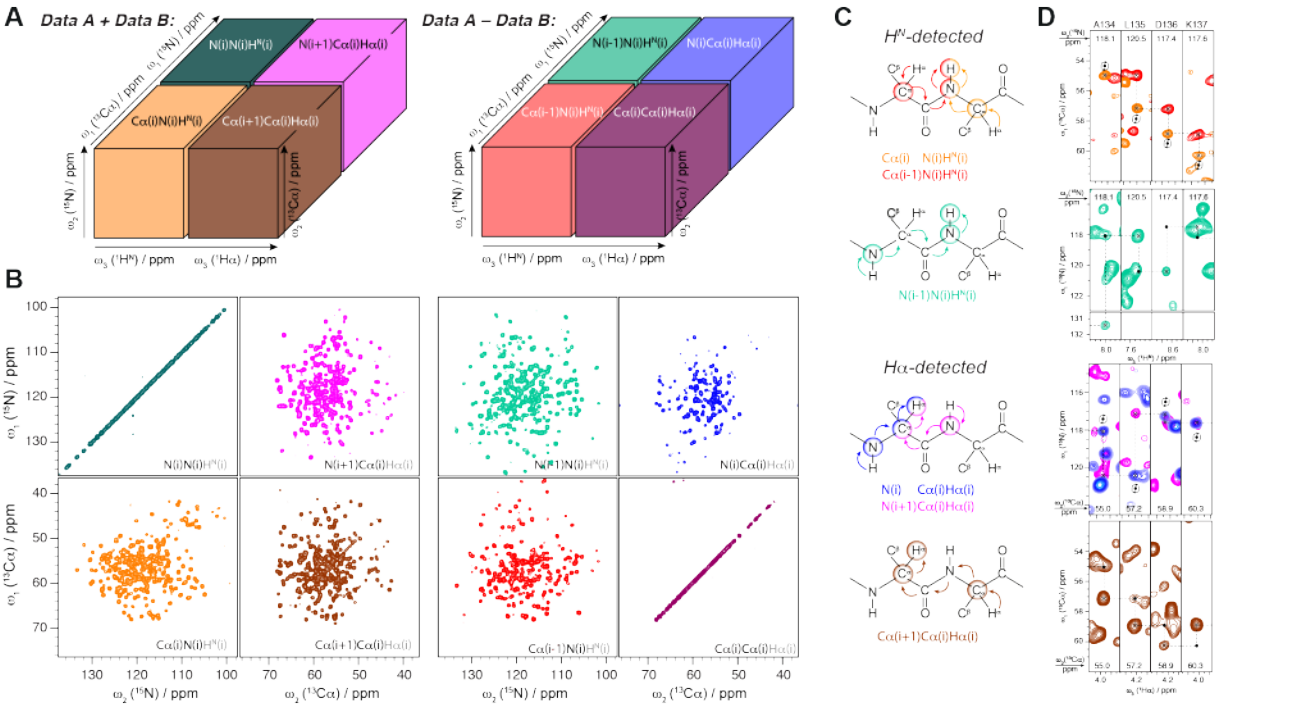

Figure 3. (A) The data layout of 8 simultaneously acquired spectra after addition/subtraction of interleaved signals A and B. Separation of pathways undergoing either $^{13}C\alpha$ or ^{15}N evolution in ω_1 is achieved by doubled spectral window and TPPI-type up- and downfield frequency shift, while separation in ω_2 is unnecessary since the frequency range ($^{13}C\alpha$ or ^{15}N) is implied from the detected nucleus. (B) Skyline projections of the 8 spectra onto the ω_1-ω_2 plane ($^{13}C\alpha$ or ^{15}N, and combinations thereof). (C) Scheme of simultaneously observed coherence transfer pathways across the protein backbone that give rise to four independent resonance matching methods. (D) Representative strips showing sequential assignment of ^{15}N, $^{13}C\alpha$, $^{1}H\alpha$ and $^{1}H^{N}$ resonances of residues A134-K137 of MBP based on intra- (*orange* and *blue* contours) and interresidue correlations (*red* and *magenta* contours) correlations found in six simultaneously acquired 3D spectra employing $^{1}H^{N}$-detection (two top panels, in *orange*, *red* and *light green*) or $^{1}H\alpha$-detection (two bottom panels, in *blue*, *magenta* and *brown*). For (H)N(CA)(CO)NH (2nd from the top) and (H)CA(N)(CO)CAHA (bottom last) spectra the implied positions of diagonal peaks (suppressed in these experiments) are shown with dots to illustrate the sequential walk. The ω_1 (either $^{13}C\alpha$ or ^{15}N)-$\omega_3(^{1}H)$ cross-sections of 3D spectra are shown at the ω_2 (either ^{15}N or $^{13}C\alpha$) frequency indicated in each strip.

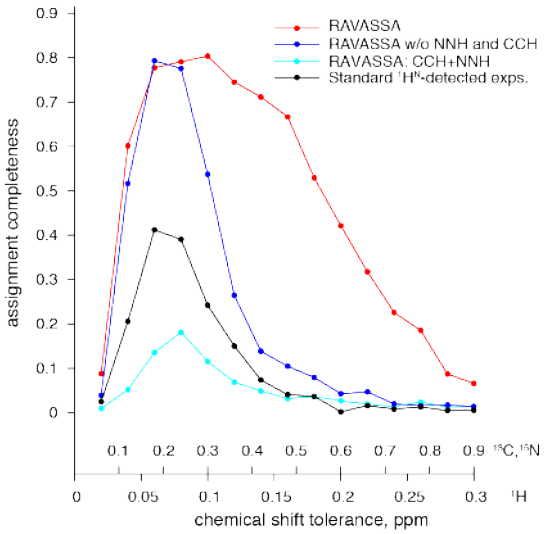

Figure 4. Characterization of the sensitivity of the automated assignment with respect to the matching tolerance. Red, blue, cyan and black dots indicate the assignment completeness, defined as the ratio of strongly assigned to all $^{1}H^{N}$, $^{1}H\alpha$, $^{13}C\alpha$, $^{13}C\beta$ and ^{15}N resonances, obtained with the compete and reduced RAVASSA datasets, as well as with the classical $^{1}H^{N}$ detected datasets,[1] respectively. Points are connected for eye guidance only.

assignment of larger proteins (since assignment ambiguity is determined by matching tolerances *and* protein size).

Figure 5 summarizes the automatically obtained resonance assignment, which is evenly distributed among different structural elements of MBP. About 18% of α and amide ^{1}H remained unassigned, which are likely undetectable with CP-based methods due to either increased local dynamics or intermediate conformational exchange as suggested by peak counts in the triple resonance spectra (see SI). In lieu of manual verification of the assignment we performed an unbiased correlation of protein dihedral angles φ and ψ predicted by TALOS-N[39] based on the automatically assigned shifts with respect to those in the X-ray derived structure (PDB 1ANF). A very good agreement (Figure 5D) proves validity of chemical shifts, whereas a very few outliers (1.5% of 470 angles) remain well within the limitations of TALOS predictions. We observe a very good match overall between the newly assigned chemical shifts and those of MBP in solution, at least for what concerns $^{13}C\alpha$ and $^{13}C\beta$ nuclei (Figure S13). Larger differences are observed for amide ^{15}N and ^{1}H, which are notoriously sensitive to the chemical environment, and vary significantly with the ligand complexation state of the protein and with preparations conditions (pH, buffer, precipitant).

In comparison with assignment strategies developed for protein solutions, the solid-state samples present unique challenges. While in solution, a main limitation to tackling larger proteins arises due to the decreased sensitivity of slowly tumbling molecules, which is inherently dependent upon particle size. The size limit in solution can, to a certain degree, be extended by increasing temperature, reducing relaxation via deuteration, as well as implementation of TROSY techniques that select for long-lived spin components.[40] While these issues are absent in the solid, the linewidths of solid protein preparations are typically larger than in solution, and unsurprisingly, the limitation in this case becomes resonance overlap and ambiguity in sequential resonance matching. (Even with the advantages of proton detection, the sensitivity at present limits acquisitions to 3D or 4D datasets, with 3D data being the most common.) The present approach using a large number of co-acquired spectra meets these unique challenges encountered in solid protein preparations.

CONCLUSION

We have described a novel strategy for backbone NMR assignment of large proteins that does not rely on deuteration, but instead is based on automated analysis of high-resolution proton detected 3D spectra obtained at ultrafast MAS with parallel $^{1}H^{N}$ and $^{1}H\alpha$-detection. We showed that full occupation of proton sites

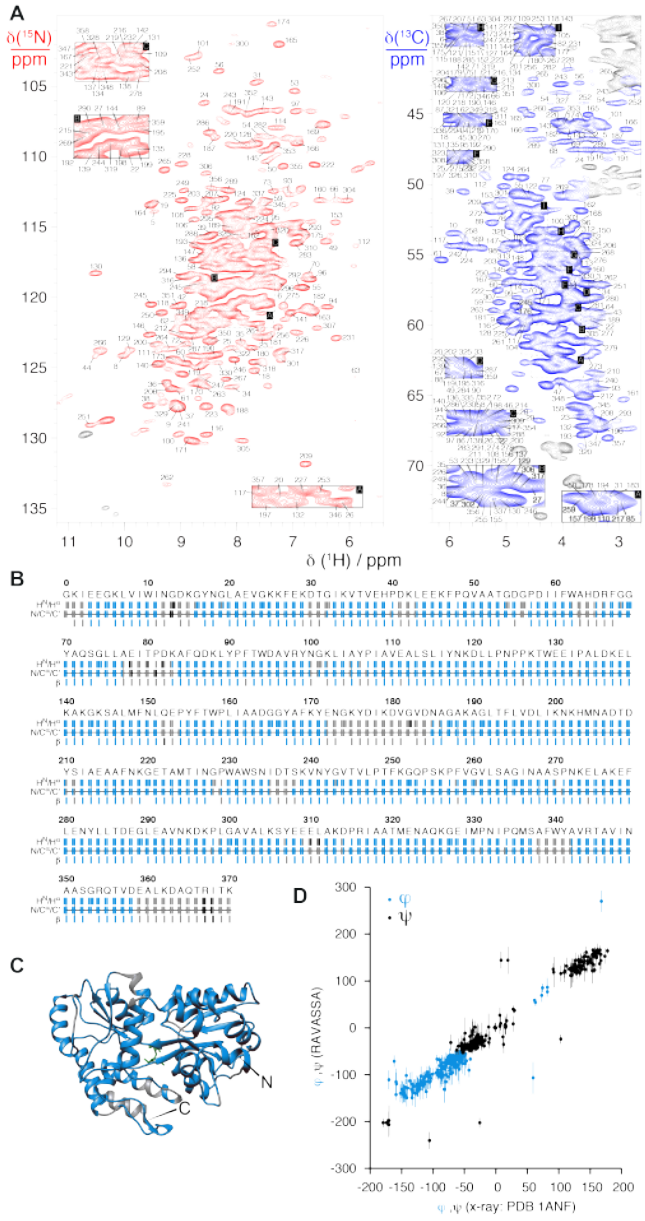

Figure 5. Assigned dipolar heteronuclear correlation spectrum of maltose binding protein: ^{15}N-^{1}H (*red* contours) and α-region of ^{13}C-^{1}H correlations (*blue* contours), acquired simultaneously. (B) Result of automated FLYA resonance assignment of MBP. Resonances with "strongly" determined chemical shifts are marked in blue (or in black, if located in isolated short fragments and thus discarded), while those below confidence threshold are shown in grey. (C) X-ray derived structural model of maltose binding protein (PDB 1ANF) with assigned residues marked in blue. (D) Backbone dihedral angles φ and ψ predicted based on assigned chemical shifts and in the X-ray structure.

enables a simultaneous acquisition of six different correlation spectra, which offers significant time savings, or equivalently, sensitivity gains. Inherent consistency and redundancy of the data provides an additional benefit to automatic resonance assignment of otherwise overwhelming complexity, as shown on the example of maltose binding protein (371 residues), which to our knowledge is the largest monomeric protein assigned in the solid state. A single uniformly ^{13}C, ^{15}N-labelled sample (< 1 mg), and approximately one week of 800 MHz NMR instrument time, using a standard single receiver, were used in this study. We furthermore showed that the assignment strategy is particularly robust against the choice of chemical shift matching tolerance, or linewidths observed for a particular sample. We therefore expect that the approach will open an efficient avenue to access site-specific NMR information in large proteins, and will be readily extended to even larger proteins, or proteins exhibiting more challenging resolution.

EXPERIMENTAL SECTION

Sample preparation

^{13}C,^{15}N-labeled N-terminal His-TEV-tagged Maltose Binding Protein (MalE 27-396, *E. coli*) was expressed in *E. coli* C41 cells and purified on a 5 ml Ni^{2+}-sepharose column (GE Healthcare) using standard methods. The His-tag was removed with TEV-Protease (in-house production) and MBP further purified by size exclusion and ion exchange chromatography. Eventually, the protein was dialyzed against 10 mM HEPES pH 7.5, 1 mM maltose. Small platelet-like crystals were produced by sitting drop vapor diffusion in 24-well plates using 600 µl reservoir (10 mM HEPES pH 7.5, 3 M $(NH_4)_2SO_4$). In each well, 15 µl MBP solution (c = 5 mg/ml) was mixed with 15 µl reservoir. Crystals grew at room temperature within 3 days. One 24-well plate yielded sufficient material for one NMR sample. $(NH_4)_2SO_4$ was chosen as precipitant (instead of e.g. PEG) in order to avoid introduction of naturally abundant ^{13}C nuclei. MBP crystals were packed by ultracentrifugation at 100,000 × *g* at 10 °C directly into a 0.7 mm MAS rotor using a 1.3 mm ultracentrifuge tool (Giotto Biotech).[41]

NMR spectroscopy

The experiments were performed on a Bruker AVANCE III 18.8 T spectrometer (^1H frequency of 800 MHz) using a 4-channel (HCND) 0.7 mm MAS probe. Sample rotation frequency was maintained at 107.00 ± 0.02 kHz, and the sample temperature was approximately 15 °C. Details on RF applied during CP transfers, pulse program listings and RF schemes are provided in SI. All spectra were processed with nmrPipe[42] using scripts provided in the SI, peak-picked automatically and converted to Xeasy format in CcpNmr Analysis 2.4.[34]

SIM-CP simulations

Simulations of simultaneous $^1H \rightarrow {}^{13}C,{}^{15}N$ CP were performed with SIMPSON[43] software version 4.0.0c for rotation frequencies between 20 and 125 kHz. Powder averaging was performed with 168×17=2856 Euler angles $\{\alpha_{MR}, \beta_{MR}, \gamma_{MR}\}$ that described the orientation of the molecule in the rotor frame. 168 angle pairs $\{\alpha_{MR}, \beta_{MR}\}$ were selected according to the Repulsion method,[44] whereas 17 γ_{MR} angles were regularly stepped from 0 to 360°. 7 spins were considered to simulate proton bath in the fully protonated proteins: $^1H^N$, $^1H\alpha$, $^1H\beta_2$, $^1H\beta_3$, ^{15}N, $^{13}C\alpha$, $^{13}C\beta$. The simulation was performed at 18.8 T magnetic field strength (^1H frequency of 800 MHz). The RF irradiation of ^{15}N, $^{13}C\alpha$ was considered on resonance, $^{13}C\beta$ was assumed -20 ppm off-resonance, and $^1H^N$, $^1H\alpha$, $^1H\beta_2/^1H\beta_3$ chemical shift offset with respect to RF carrier (typically 4.7 ppm for solvent signal) was set to 4.0, -0.5 and -2.2 ppm, respectively. Chemical shift anisotropy was neglected for all spins. RF irradiation strength ranges were 0-250 kHz for ^1H, ^{13}C and ^{15}N. RF field inhomogeneity was neglected, thus constant RF amplitude was assumed during CP. Only proton thermally equilibrated magnetization was considered at the starting point of the simulation. To simulate CP transfer the propagator for one rotor period was calculated and reused to reach contact time of 300 µs. The SIM-CP efficiency was evaluated as the ^{15}N and $^{13}C\alpha$ magnetization at the end of RF irradiation. Further details, including geometry of the restricted spin system and sample scripts, can be found in SI.

Automated assignment

Automated analysis of obtained correlations was performed by FLYA as implemented in CYANA package v. 3.98.5. Library extensions for new types of experiments as well as CYANA batch scripts are provided in SI. Optimal assignment was obtained using matching tolerances of 0.1, 0.3 and 0.3 ppm for ^1H, ^{13}C and ^{15}N frequencies, respectively. A population size of 50 was set for genetic optimization algorithm. 20 independent runs were performed to identify consensus chemical shifts, with a threshold of 16 self-consistent chemical shift values for a "strong" assignment. Detailed statistics on the assignment completeness for particular nuclei and peak lists are provided in SI.

ASSOCIATED CONTENT

Supporting Information

Detailed NMR experimental setup, radiofrequency irradiation schemes with Bruker spectrometer implementation, details on data processing and automated analysis (PDF). The Supporting Information is available free of charge on the ACS Publications website.

AUTHOR INFORMATION

Corresponding Author

Guido Pintacuda (guido.pintacuda@ens-lyon.fr)

Author Contributions

‡These authors contributed equally.

Notes

The authors declare no competing financial interests.

ACKNOWLEDGMENT

The MBP plasmid was kindly provided by Prof. Gottfried Otting (ANU). The work was funded by the European Research Council (ERC) under the European Union's Horizon 2020 research and innovation programme (ERC-2015-CoG GA 648974). JS was supported with the European Commission's REA with a MSCA fellowship (GA 661799) and by the Polish National Agency for Academic Exchange (contract No PPN/PPO/2018/1/00098). The computational resources were provided by the Polish Infrastructure for Supporting Computational Science in the European Research Space (PLGRID).

REFERENCES

(1) Barbet-Massin, E.; Pell, A. J.; Retel, J. S.; Andreas, L. B.; Jaudzems, K.; Franks, W. T.; Nieuwkoop, A. J.; Hiller, M.; Higman, V.; Guerry, P.; Ber- tarello, A.; Knight, M. J.; Felletti, M.; Le Marchand, T.; Kotelovica, S.; Akopjana, I.; Tars, K.; Stoppini, M.; Vittorio, B.; Bolognesi, M.; Ricagno, S.; Chou, J. J.; Griffin, R. G.; Oschkinat, H.; Lesage, A.; Emsley, L.; Herrmann, T.; Pintacuda, G. Rapid proton-detected NMR assignment for proteins with fast magic angle spinning*; J. Am. Chem. Soc.* **2014**, *136*, 12489-12497.

(2) Ishii, Y.; Yesinowski, J. P.; Tycko, R. Sensitivity enhancement in solid-state 13C NMR of synthetic polymers and biopolymers by 1H NMR detection with high-speed magic angle spinning*; J. Am. Chem. Soc.* **2001**, *123*, 2921-2922.
(3) Reif, B.; Jaroniec, C. P.; Rienstra, C. M.; Hohwy, M.; Griffin, R. G. 1H-1H MAS correlation spectroscopy and distance measurements in a deuterated peptide*; J. Magn. Reson.* **2001**, *151*, 320-327.
(4) Paulson, E. K.; Morcombe, C. R.; Gaponenko, V.; Dancheck, B.; Byrd, R. A.; Zilm, K. W. Sensitive high resolution inverse detection NMR spectroscopy of proteins in the solid state*; J. Am. Chem. Soc.* **2003**, *125*, 15831-15836.
(5) Zhou, D. H.; Shea, J. J.; Nieuwkoop, A. J.; Franks, W. T.; Wylie, B. J.; Mullen, C.; Sandoz, D.; Rienstra, C. M. Solid-state protein-structure determination with proton-detected triple-resonance 3D magic-angle-spinning NMR spectroscopy*; Angew. Chem. Int. Ed. Engl.* **2007**, *46*, 8380-8383.
(6) Andreas, L. B.; Le Marchand, T.; Jaudzems, K.; Pintacuda, G. High-resolution proton-detected NMR of proteins at very fast MAS*; J. Magn. Reson.* **2015**, *253*, 36-49.
(7) Böckmann, A.; Ernst, M.; Meier, B. H. Spinning proteins, the faster, the better?*; J. Magn. Reson.* **2015**, *253*, 71-79.
(8) Samoson, A. H-Mas*; J. Magn. Reson.* **2019**, *306*, 167-172.
(9) Knight, M. J.; Webber, A. L.; Pell, A. J.; Guerry, P.; Barbet-Massin, E.; Bertini, I.; Felli, I. C.; Gonnelli, L.; Pierattelli, R.; Emsley, L.; Lesage, A.; Herrmann, T.; Pintacuda, G. Fast resonance assignment and fold determination of human superoxide dismutase by high-resolution proton-detected solid-state MAS NMR spectroscopy*; Angew. Chem. Int. Ed. Engl.* **2011**, *50*, 11697-11701.
(10) Lewandowski, J. R.; Dumez, J. N.; Akbey, Ü.; Lange, S.; Emsley, L.; Oschkinat, H. Enhanced resolution and coherence lifetimes in the solid-state NMR spectroscopy of perdeuterated proteins under ultrafast Magic-Angle Spinning*; J. Chem. Phys. Lett.* **2011**, *2*, 2205-2211.
(11) Andreas, L. B.; Jaudzems, K.; Stanek, J.; Lalli, D.; Bertarello, A.; Le Marchand, T.; De Paepe, D. C.; Kotelovica, S.; Akopjana, I.; Knott, B.; Wegner, S.; Engelke, F.; Lesage, A.; Emsley, L.; Tars, K.; Herrmann, T.; Pintacuda, G. Structure of fully protonated proteins by proton-detected magic-angle spinning NMR*; Proc. Natl. Acad. Sci. USA* **2016**, *113*, 9187-9192.
(12) Struppe, J.; Quinn, C. M.; Lu, M.; Wang, M.; Hou, G.; Lu, X.; Kraus, J.; Andreas, L. B.; Stanek, J.; Lalli, D.; Lesage, A.; Pintacuda, G.; Maas, W.; Gronenborn, A. M.; Polenova, T. Expanding the horizons for structural analysis of fully protonated protein assemblies by NMR spectroscopy at MAS frequencies above 100 kHz*; Solid State Nucl. Magn. Reson.* **2017**, *87*, 117-125.
(13) Marchanka, A.; Stanek, J.; Pintacuda, G.; Carlomagno, T. Rapid access to RNA resonances by proton-detected solid-state NMR at >100 kHz MAS*; Chem. Commun.* **2018**, *54*, 8972-8975.
(14) Penzel, S.; Smith, A. A.; Agarwal, V.; Hunkeler, A.; Org, M. L.; Samoson, A.; Böckmann, A.; Ernst, M.; Meier, B. H. Protein resonance assignment at MAS frequencies approaching 100 kHz: a quantitative comparison of J-coupling and dipolar-coupling-based transfer methods*; J. Biomol. NMR* **2015**, *63*, 165-186.
(15) Andreas, L. B.; Stanek, J.; Le Marchand, T.; Bertarello, A.; Paepe, D. C.; Lalli, D.; Krejcikova, M.; Doyen, C.; Oster, C.; Knott, B.; Wegner, S.; Engelke, F.; Felli, I. C.; Pierattelli, R.; Dixon, N. E.; Emsley, L.; Herrmann, T.; Pintacuda, G. Protein residue linking in a single spectrum for magic-angle spinning NMR assignment*; J. Biomol. NMR* **2015**, *62*, 253-261.
(16) Xiang, S.; Grohe, K.; Rovó, P.; Vasa, S. K.; Giller, K.; Becker, S.; Linser, R. Sequential backbone assignment based on dipolar amide-to-amide correlation experiments*; J. Biomol. NMR* **2015**, *62*, 303-311.
(17) Fricke, P.; Chevelkov, V.; Zinke, M.; Giller, K.; Becker, S.; Lange, A. Backbone assignment of perdeuterated proteins by solid-state NMR using proton detection and ultrafast magic-angle spinning*; Nat. Protoc.* **2017**, *12*, 764-782.
(18) Wang, S.; Munro, R. A.; Shi, L.; Kawamura, I.; Okitsu, T.; Wada, A.; Kim, S.-Y.; Jung, K.-H.; Brown, L. S.; Ladizhansky, V. Solid-state NMR spectroscopy structure determination of a lipid-embedded heptahelical membrane protein*; Nat. Meth.* **2013**, *10*, 1007-1012.
(19) Retel, J. S.; Nieuwkoop, A. J.; Hiller, M.; Higman, V. A.; Barbet-Massin, E.; Stanek, J.; Andreas, L. B.; Franks, W. T.; van Rossum, B. J.; Vinothkumar, K. R.; Handel, L.; de Palma, G. G.; Bardiaux, B.; Pintacuda, G.; Emsley, L.; Kuhlbrandt, W.; Oschkinat, H. Structure of outer membrane protein G in lipid bilayers*; Nat. Commun.* **2017**, *8*, 2073.
(20) Vasa, S. K.; Singh, H.; Rovo, P.; Linser, R. Dynamics and Interactions of a 29 kDa Human Enzyme Studied by Solid-State NMR*; J. Phys. Chem. Lett.* **2018**, *9*, 1307-1311.
(21) Ward, M. E.; Shi, L.; Lake, E.; Krishnamurthy, S.; Hutchins, H.; Brown, L. S.; Ladizhansky, V. Proton-detected solid-state NMR reveals intramembrane polar networks in a seven-helical transmembrane protein proteorhodopsin*; J. Am. Chem. Soc.* **2011**, *133*, 17434-17443.
(22) Gauto, D. F.; Estrozi, L. F.; Schwieters, C. D.; Effantin, G.; Macek, P.; Sounier, R.; Sivertsen, A. C.; Schmidt, E.; Kerfah, R.; Mas, G.; Colletier, J. P.; Güntert, P.; Favier, A.; Schoehn, G.; Schanda, P.; Boisbouvier, J. Integrated NMR and cryo-EM atomic-resolution structure determination of a half-megadalton enzyme complex*; Nat. Commun.* **2019**, *10*, 2697.
(23) Gupta, S.; Tycko, R. Segmental isotopic labeling of HIV-1 capsid protein assemblies for solid state NMR*; J. Biomol. NMR* **2018**, *70*, 103-114.
(24) Han, Y.; Ahn, J.; Concel, J.; Byeon, I.-J. L.; Gronenborn, A. M.; Yang, J.; Polenova, T. Solid-State NMR Studies of HIV-1 Capsid Protein Assemblies*; J. Am. Chem. Soc.* **2010**, *132*, 1976-1987.
(25) Stanek, J.; Andreas, L. B.; Jaudzems, K.; Cala, D.; Lalli, D.; Bertarello, A.; Schubeis, T.; Akopjana, I.; Kotelovica, S.; Tars, K.; Pica, A.; Leone, S.; Picone, D.; Xu, Z.-Q.; Dixon, N. E.; Martinez, D.; Berbon, M.; El Mammeri, N.; Noubhani, A.; Saupe, S.; Habenstein, B.; Loquet, A.; Pintacuda, G. NMR spectroscopic assignment of backbone and side-chain protons in fully protonated proteins: microcrystals, sedimented assemblies, and amyloid fibrils*; Angew. Chem. Int. Ed.* **2016**, *128*, 15730-15735.
(26) Lalli, D.; Idso, M. N.; Andreas, L. B.; Hussain, S.; Baxter, N.; Han, S.; Chmelka, B. F.; Pintacuda, G. Proton-Based Structural Analysis of a Heptahelical Transmembrane Protein in Lipid Bilayers*; J. Am. Chem. Soc.* **2017**, *139*, 13006-13012.
(27) Malmodin, D.; Papavoine, C. H.; Billeter, M. Fully automated sequence-specific resonance assignments of hetero-nuclear protein spectra*; J. Biomol. NMR* **2003**, *27*, 69-79.
(28) Niklasson, M.; Ahlner, A.; Andresen, C.; Marsh, J. A.; Lundström, P. Fast and accurate resonance assignment of small-to-large proteins by combining automated and manual approaches*; PLoS Comput. Biol.* **2015**, *11*, e1004022.
(29) Gopinath, T.; Veglia, G. Dual acquisition magic-angle spinning solid-state NMR-spectroscopy: simultaneous acquisition of multidimensional spectra of biomacromolecules*; Angew. Chem. Int. Ed. Engl.* **2012**, *51*, 2731-2735.
(30) Das, B. B.; Opella, S. J. Multiple acquisition/multiple observation separated local field/chemical shift correlation solid-state magic angle spinning NMR spectroscopy*; J. Magn. Reson.* **2014**, *245*, 98-104.
(31) Linser, R.; Bardiaux, B.; Higman, V.; Fink, U.; Reif, B. Structure calculation from unambiguous long-range amide and methyl 1H-1H distance restraints for a microcrystalline protein with MAS solid-state NMR spectroscopy*; J. Am. Chem. Soc.* **2011**, *133*, 5905-5912.
(32) Gopinath, T.; Veglia, G. Orphan spin operators enable the acquisition of multiple 2D and 3D magic angle spinning solid-state NMR spectra*; J Chem Phys* **2013**, *138*, 184201.
(33) Sharma, K.; Madhu, P. K.; Mote, K. R. A suite of pulse sequences based on multiple sequential acquisitions at one and two radiofrequency channels for solid-state magic-angle spinning NMR studies of proteins*; J. Biomol. NMR* **2016**, *65*, 127-141.
(34) Vranken, W. F.; Boucher, W.; Stevens, T. J.; Fogh, R. H.; Pajon, A.; Llinas, M.; Ulrich, E. L.; Markley, J. L.; Ionides, J.; Laue, E. D. The CCPN data model for NMR spectroscopy: development of a software pipeline*; Proteins* **2005**, *59*, 687-696.
(35) Schmidt, E.; Güntert, P. A new algorithm for reliable and general NMR resonance assignment*; J. Am. Chem. Soc.* **2012**, *134*, 12817-12829.
(36) Schmidt, E.; Gath, J.; Habenstein, B.; Ravotti, F.; Székely, K.; Huber, M.; Buchner, L.; Böckmann, A.; Meier, B. H.; Güntert, P. Automated solid-state NMR resonance assignment of protein microcrystals and amyloids*; J. Biomol. NMR* **2013**, *56*, 243-254.
(37) Pritišanac, I.; Würz, J. M.; Alderson, T. R.; Güntert, P. Automatic structure-based NMR methyl resonance assignment in large proteins*; Nat. Commun.* **2019**, *10*, 4922.
(38) Barbet-Massin, E.; Pell, A. J.; Jaudzems, K.; Franks, W. T.; Retel, J. S.; Kotelovica, S.; Akopjana, I.; Tars, K.; Emsley, L.; Oschkinat, H.; Lesage, A.; Pintacuda, G. Out-and-back 13C-13C scalar transfers in protein resonance assignment by proton-detected solid-state NMR under ultra-fast MAS*; J. Biomol. NMR* **2013**, *56*, 379-386.

(39) Shen, Y.; Bax, A. Protein backbone and sidechain torsion angles predicted from NMR chemical shifts using artificial neural networks*; J. Biomol. NMR* **2013**, *56*, 227-241.
(40) Salzmann, M.; Pervushin, K.; Wider, G.; Senn, H.; Wüthrich, K. TROSY in triple-resonance experiments: new perspectives for sequential NMR assignment of large proteins*; Proc. Natl. Acad. Sci. U. S. A.* **1998**, *95*, 13585-13590.
(41) Bertini, I.; Engelke, F.; Gonnelli, L.; Knott, B.; Luchinat, C.; Osen, D.; Ravera, E. On the use of ultracentrifugal devices for sedimented solute NMR*; J. Biomol. NMR* **2012**, *54*, 123-127.
(42) Delaglio, F.; Grzesiek, S.; Vuister, G. W.; Zhu, G.; Pfeifer, J.; Bax, A. NMRPipe: a multidimensional spectral processing system based on UNIX pipes*; J. Biomol. NMR* **1995**, *6*, 277-293.
(43) Bak, M.; Rasmussen, J. T.; Nielsen, N. C. SIMPSON: a general simulation program for solid-state NMR spectroscopy*; J. Magn. Reson.* **2000**, *147*, 296-330.
(44) Bak, M.; Nielsen, N. C. REPULSION, A Novel Approach to Efficient Powder Averaging in Solid-State NMR*; J. Magn. Reson.* **1997**, *125*, 132-139.

Supporting Information

Automated backbone NMR resonance assignment of large proteins using redundant linking from a single simultaneous acquisition

Jan Stanek,[#,‖,‡] Tobias Schubeis,[#,‡] Piotr Paluch,[‖] Peter Güntert,[&,§,=] Loren B Andreas,[#,⊥] and Guido Pintacuda[#,*]

[#]Centre de RMN à Très Hauts Champs, FRE (FRE 2034 CNRS, UCB Lyon 1, ENS Lyon), Université de Lyon, 5 rue de la Doua, 69100 Villeurbanne, France; [‖]Faculty of Chemistry, University of Warsaw, 02089 Warsaw, Poland; [⊥]Max Planck Institute for Biophysical Chemistry, Am Fassberg 11, D-37077 Göttingen, Germany, [&]Physical Chemistry, Eidgenössische Technische Hochschule Zurich, Zurich, Switzerland; [§]Center for Biomolecular Magnetic Resonance, Institute of Biophysical Chemistry, Goethe University Frankfurt, Frankfurt, Germany; [=]Department of Chemistry, Tokyo Metropolitan University, Hachioji, Japan

CONTENTS

A. Simultaneous CP under ultrafast MAS

The contribution of amide and aliphatic proton to ^{15}N and ^{13}C pathways in conventional ^{15}N- and ^{13}C-CP-HSQC experiments is tracked in Figure S1 by frequency encoding the source proton. It can be seen that the two $^{1}H^{N}\rightarrow^{15}N$ and $^{1}H\alpha\rightarrow^{13}C\alpha$ paths are nearly independent, with for example only about 7 percent of the signal in Fig S1B originating from amide protons (Box B4). In S1A, box A1 and A2, it can be seen that about 13 percent of the signal in the H-N-H transfer pathway originates from aliphatic protons and about 5 percent from alpha protons. Lost magnetization in the final CP (Boxes A4 and B1) is also minimal, and is not included in the determination of total signal. Note that this magnetization leak occurs irrespective of whether conventional or simultaneous CP is performed, and is generally related to the "cross-talk" between pathways (i.e. $^{15}N\rightarrow^{1}H$aliphatic and $^{13}C\alpha\rightarrow^{1}H^{N}$ transfers).

At 100 kHz MAS, we observed a 6 and 16% loss, respectively, in the simultaneous experiments as compared with conventional ^{13}C- and ^{15}N-CP-HSQC spectra recorded separately (Figure S3). The negligible loss for the ^{13}C pathway, and the larger loss for ^{15}N are in full agreement with previous reports for SIM-CP with heteronuclear detection at slow MAS.[1] A somewhat larger impact of SIM-CP for ^{15}N is fully confirmed by quantum-mechanical simulations[2] on a system of 7 spins (Figure S2). These simulations highlight that the ^{15}N spins are sensitive to drainage of $^{1}H\alpha$ (and other aliphatic) polarization during concurrent ^{1}H-^{13}C CP, while for $^{13}C\alpha$, abundant remote side-chain protons constitute a better polarization reservoir.

Figure S4 shows the performance of ^{1}H-^{13}C and ^{1}H-^{15}N (independent) CP transfers measured as the largest magnitude in ^{13}C- and ^{15}N-CP-HSQC 1D experiments as a function of ^{1}H and ^{13}C, or ^{1}H and ^{15}N RF strengths, respectively. This proves that both CPs exhibit optimal efficiency for analogous conditions, and simultaneous ^{1}H-^{13}C,^{15}N CP, which requires a common ^{1}H RF field strength for both transfers, does not compromise their efficiency.

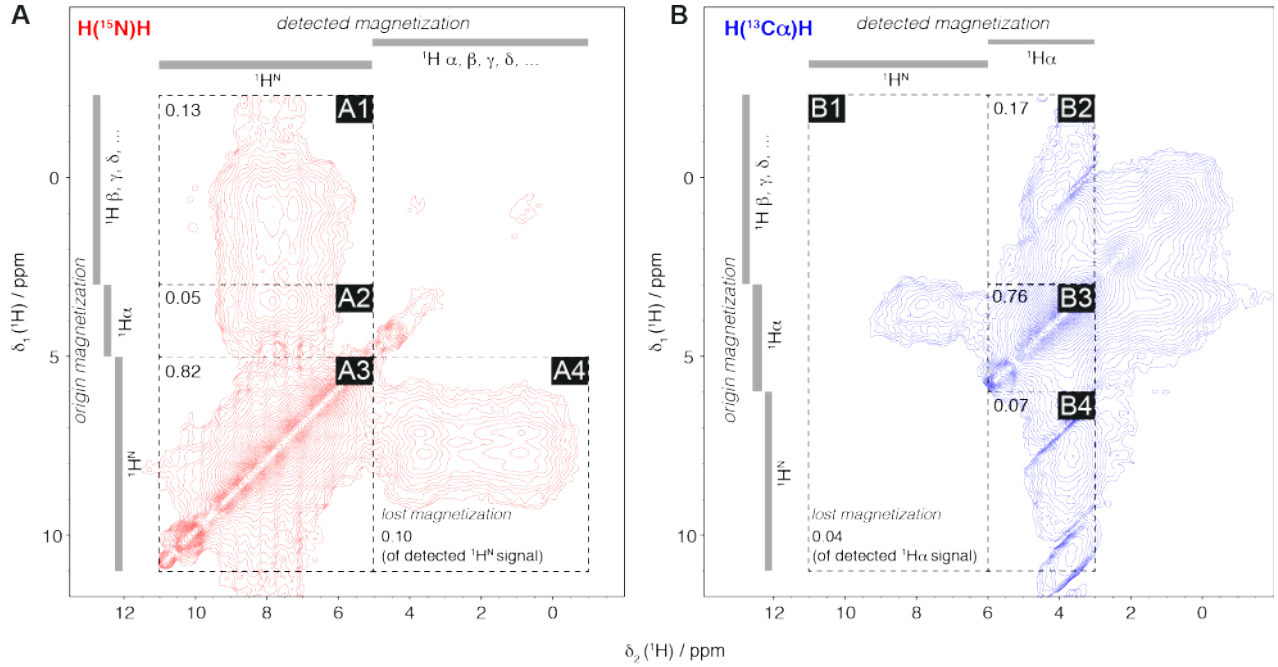

Figure S1. Investigation of the degree of independence and interference during simultaneous CP by recording the source proton in normally acquired 2D H(N)H and H(C)H spectra. Optimized contact times of *forward* CP were 1100 µs ($^{1}H\rightarrow^{15}N$) and 400 µs ($^{1}H\rightarrow^{13}C$), and of *backward* CP were 900 µs ($^{15}N\rightarrow^{1}H$) and 200 µs ($^{13}C\rightarrow^{1}H$) were used.

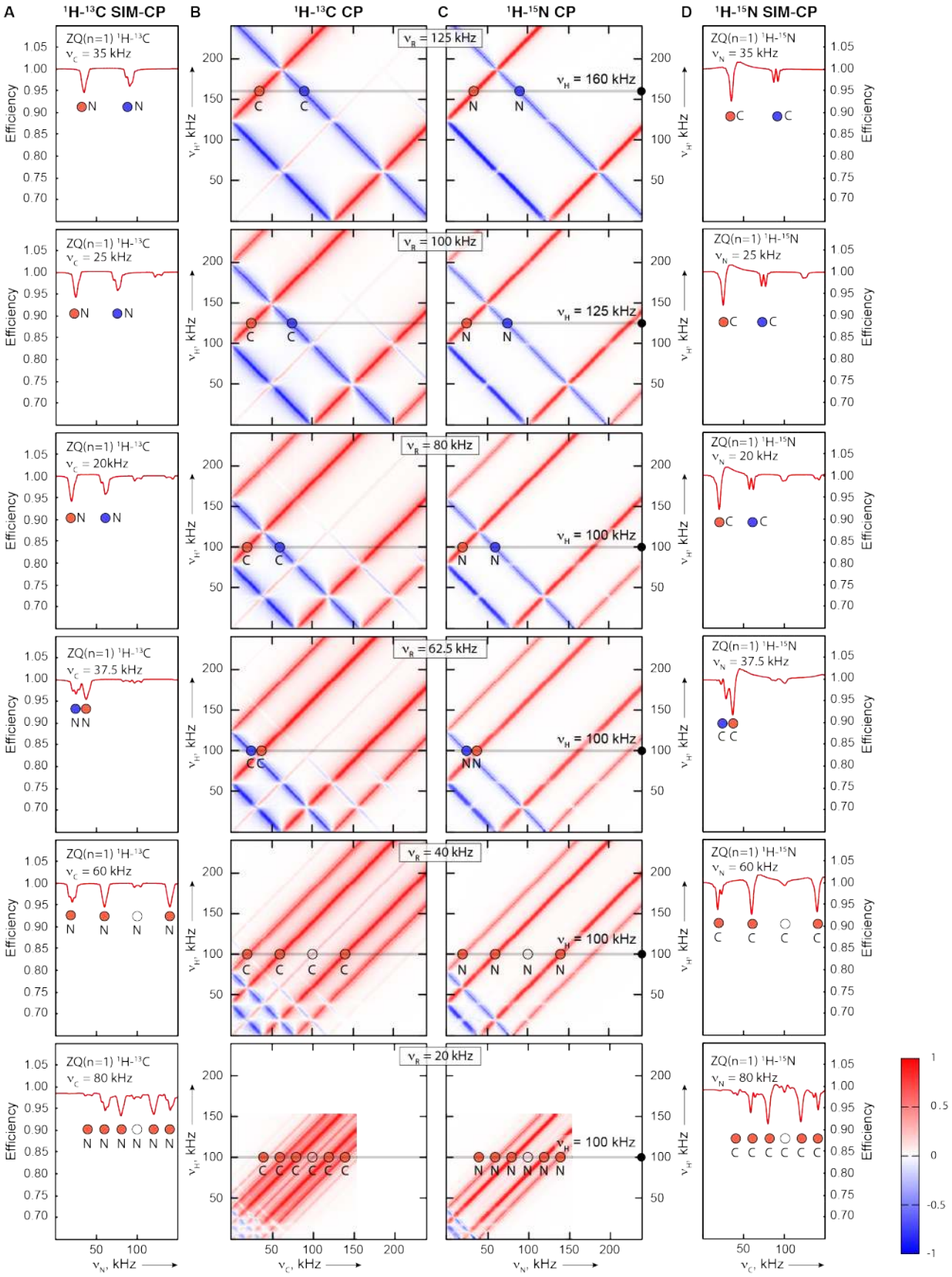

Figure S2. SIMPSON simulations that characterize interference occurring during simultaneous CP, leading to minor loss of transfer efficiency. The simulations were performed for ^{1}H-^{13}C (A, B) and ^{1}H-^{15}N CP (C, D) with ^{13}C or ^{15}N detection. Simulation of ^{1}H-^{13}C or ^{15}N CP transfer efficiency is shown in various conditions of different spinning frequencies (ν_R) equal to 125, 100, 80, 62.5, 40, 20 kHz. In the case of simulation at ν_R=20kHz, an RF field of up to only 160 kHz was considered due to general probe limitation when operating typical devices that spin at this frequency. A) Simultaneous ^{1}H-^{13}C/^{1}H-^{15}N CP with ^{13}C detection as a function of ν_{15N} and constant ν_{1H} and ν_{13C}, B)

Dual channel (conventional) ^{1}H-^{13}C CP as a function of ν_{1H} and ν_{13C} , C) Dual channel ^{1}H-^{15}N CP as function of ν_{1H} and ν_{15N}, D) Simultaneous ^{1}H-^{13}C/^{1}H-^{15}N CP with ^{15}N detection as a function of ν_{13C} and constant ν_{1H} and ν_{15N} . In A) and D), a slight decrease (up to 8%) in transfer efficiency is observed when the ^{15}N or ^{13}C RF reaches an effective simultaneous CP matching condition with the proton RF. These conditions are indicated with red and blue dots, according to whether the simultaneous CP is a zero- or double-quantum condition, and labeled with the nucleus name (“C” or “N”).

Listing 1. Sample SIMPSON input for simulation of simultaneous CP (SIM-CP).

```
#1H-13C CP efficiency simulation as a function of 1H and 13C RF
#for 7 spin system (Ca, Cb, N, NH, HA, HB HB')
#parametrs B0=800MHz RO=100kHz crysl_fle=rep168 gamma=17
#with dt=0.1 it is important for long pulse
#PPaluch CBMM PAN Lodz 2019
#PPaluch CNBCH UW Warszawa 2019
# piotr.paluch@gmail.com
spinsys {
#      1      2      3      4      5      6      7
#    1C1    2C2    3N3    4H4    5H5    6H6    7H7
# 1) C1 CA
# 2) C2 CB
# 3)  N3 N
# 4) H4 NH
# 5) H5 HA
# 6) H6 CB
# 7) H7 CB'
 channels 13C 15N 1H
 nuclei   13C 13C 15N 1H 1H 1H 1H

 shift 1 0 0 0 0 0 0
 shift 2 -20.0p 0 0 0 0 0
 shift 3 0 0 0 0 0 0
 shift 4 4.0p 0 0 0 0 0
 shift 5 -0.5p 0 0 0 0 0
 shift 6 -2.2p 0 0 0 0 0
 shift 7 -2.2p 0 0 0 0 0

 dipole 1 2 -2041.67 0 102.41 -87.463
 dipole 1 3 981.8 0 113.86 153.22
 dipole 1 4 -3178.8 0 137.43 148.67
 dipole 1 5 -25134 0 5.1219 131.58
 dipole 1 6 -2880.2 0 92.697 -62.075
 dipole 1 7 -3039.6 0 84.796 -109.45

 dipole 2 3 202.13 0 95.985 120.8
 dipole 2 4 -1271.2 0 115.26 119.77
 dipole 2 5 -3207 0 48.769 94.695
 dipole 2 6 -24653 0 77.589 -23.695
 dipole 2 7 -24683 0 60.422 -146.98

 dipole 3 4 12939 0 171.41 102.23
 dipole 3 5 1374.6 0 37.115 -25.169
 dipole 3 6 309.25 0 81.753 -48.817
 dipole 3 7 567.95 0 73.565 -79.622

 dipole 4 5 -4712.4 0 27.139 -30.137
 dipole 4 6 -2211.4 0 67.374 -49.978
 dipole 4 7 -3301.1 0 58.021 -79.526

 dipole 5 6 -7175.8 0 117.02 -61.512
 dipole 5 7 -9219.2 0 111.54 -107.28

 dipole 6 7 -21864 0 80.277 -177.13
}

par {
  method dsyev
  proton_frequency 800e6
  spin_rate        1.0e5
  gamma_angles          17
  np              1
  sw               spin_rate
  crystal_file     rep168
  start_operator   I4x+I5x+I6x+I7x
```

```
  detect_operator  I1p
  verbose          0000
  variable RF_H 0
  variable RF_C 0
  variable RF_N 0
  ######
  variable CT_us 300.0

  variable RF_H_min 0.0
  variable RF_H_max 240000.0
  variable RF_H_step 240

  variable RF_C_min 0.0
  variable RF_C_max 240000.0
  variable RF_C_step 240
}

proc pulseq {} {
  global par
  maxdt 0.1
  set Tr [expr 1.0e6/$par(spin_rate)]
  set nTr [expr int($par(CT_us)/$Tr)]
    reset
    pulse $Tr $par(RF_C) 0 $par(RF_N) 0 $par(RF_H) 0
    store 1

    reset
    prop 1 $nTr
    acq
  }

proc main {} {
  global par
  foreach par(spin_rate) {100000.0 } {
  set FileRe_Im_Abs [open "$par(name).res" w]
  for {set a 0} {$a<=$par(RF_H_step)} {incr a} {
  set par(RF_H)  [expr $par(RF_H_min)+$a*($par(RF_H_max)-$par(RF_H_min))/$par(RF_H_step)]
  for {set b 0} {$b<=$par(RF_C_step)} {incr b} {
    set par(RF_C)  [expr $par(RF_C_min)+$b*($par(RF_C_max)-$par(RF_C_min))/$par(RF_C_step)]
    set f [fsimpson]
    set Sr [findex $f 1 -re]
    set Si [findex $f 1 -im]
    puts  $FileRe_Im_Abs "[expr  $par(RF_H)/1.0e3]  [expr  $par(RF_C)/1.0e3]  [expr  $Sr]  [expr  $Si]
  [expr sqrt($Sr**2+$Si**2)]"
    funload $f
    }
    puts $FileRe_Im_Abs " "
    }
   close $FileRe_Im_Abs
   }
   }
```

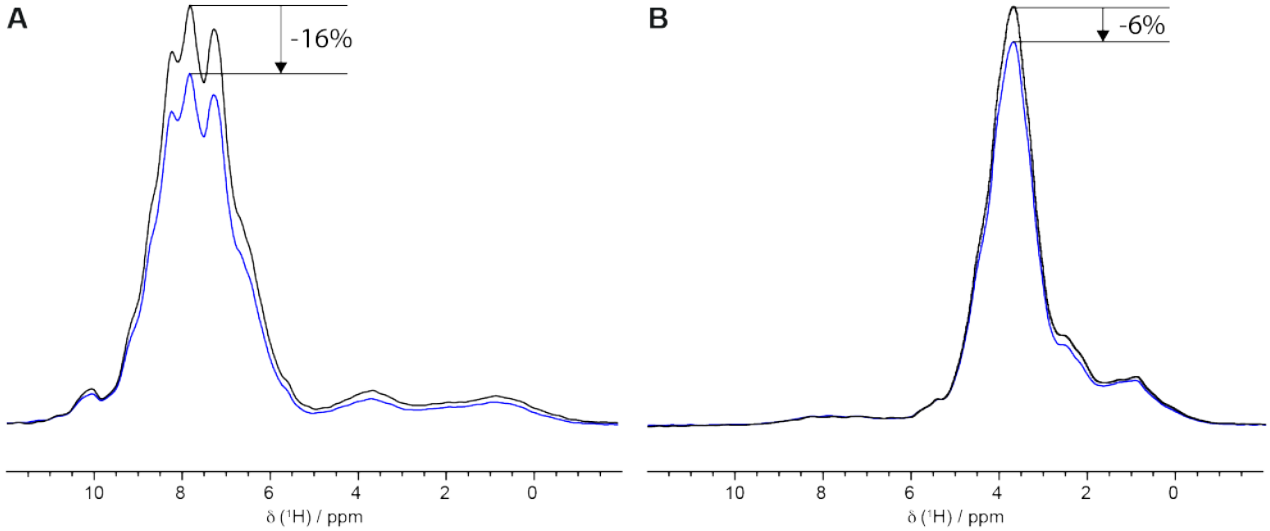

Figure S3. Quantification of interference between $^{1}H \rightarrow ^{15}N$ and $^{1}H \rightarrow ^{13}C$ CP at 107 kHz MAS on a sample of uniformly ^{13}C,^{15}N-labeled maltose binding protein. (A) 1D (H)NH experiment recorded with (in blue) and without (in black) simultaneous irradiation of ^{13}C nuclei. (B) 1D (H)CH experiment with a $^{13}C\alpha$-selective refocusing pulse recorded with (in blue) and without (in black) simultaneous irradiation of ^{15}N nuclei. ^{15}N and ^{13}C RF irradiation was applied for the same time in all cases (800 μs).

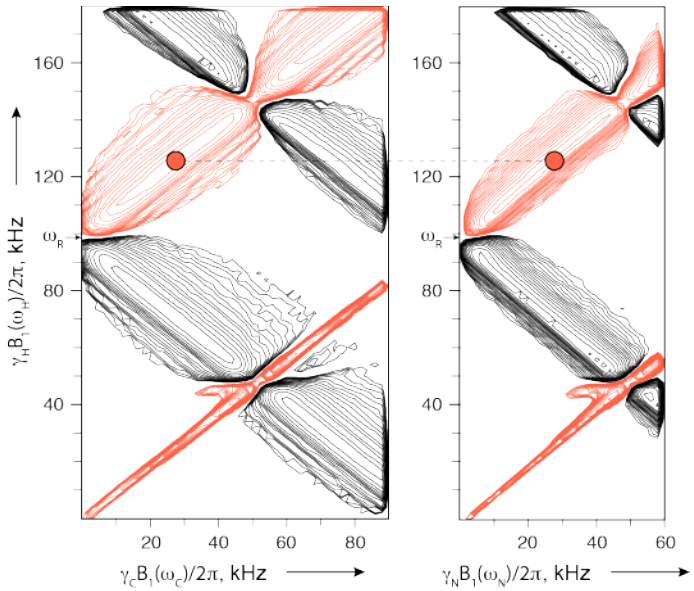

Figure S4. Standard (sequential) CP conditions for ^{1}H-^{13}C (left) and ^{1}H-^{15}N CP (right) at 107 kHz MAS in a 0.7 mm Bruker HCN probe on a 800 MHz spectrometer. Signal intensity was evaluated by stepwise variation of ^{1}H and either ^{13}C or ^{15}N RF strength during a fixed contact time CP following the first ^{1}H pulse in a 1D (H)CH or (H)NH experiment ("first FID"). The intensities along detected ^{1}H dimension were summed over the aliphatic or amide ^{1}H range. Zero-quantum (ZQ) and double-quantum (DQ) CP show opposite signs and are shown in red and black, respectively. Red disks connected by a horizontal dashed line (i.e. at common ^{1}H RF strength) indicate the optimal CP conditions for both sequential transfers, which are chosen here for the simultaneous CP (SIM-CP).

B. Detailed RF pulse schemes

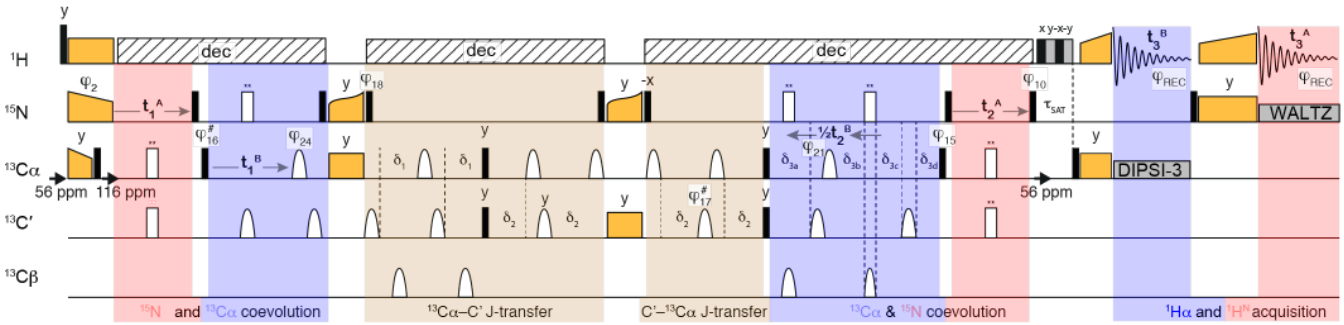

Figure S5. Radiofrequency (RF) pulse scheme for the "8-in-1" experiment. Heteronuclear cross-polarization (CP) transfers are shown as either wide rectangular, trapezoid or tangential orange shapes simultaneously on two or three RF channels. RF strength, duration and detailed shapes for CP transfers are provided in Table S2. Solid and open pulses represent high-power 90° and 180° pulses, respectively. Open pulses marked with double star (**) denote composite 180° pulses $90_x°180_y°90_x°$, which were used to minimize signal losses on the pathways other than the decoupled one. In our implementation (see Section J) these pulses are optional, and can be skipped for short evolution times. Open bell shapes on ^{13}C channels represent Q3[3] (for ^{13}Cα and ^{13}C′) and ReBURP[4] (for ^{13}Cβ) selective pulses. Pulse durations and peak RF strength were 161.5, 178.5 and 960.9 μs and 20.43, 18.49 and 6.52 kHz for ^{13}Cα, ^{13}C′ and ^{13}Cβ pulses respectively. Note that the moderately selective ^{13}Cα pulses affect both ^{13}Cα and ^{13}Cβ spins. Heteronuclear ^{1}H decoupling during indirect evolution or *J*-transfer periods is shown in hatched grey. Swept-TPPM[5-6] ^{1}H decoupling with RF field of 10 kHz and pulse length of 25 μs was used. WALTZ-16[7] and DISPI-3[8] with RF strength of 10 and 20 kHz, and pulse lengths of 25 and 12.5 μs, were used for ^{15}N and ^{13}C decoupling during signal acquisition, respectively. The MISSISSIPPI water suppression,[9] with duration τ_{SAT} of 200 ms and RF strength of 25.4 kHz, is shown as a composite block of four solid and grey pulses. Relaxation-optimized ^{13}Cα–^{13}C′ *J*-transfer delays δ_1 and δ_2 were 4.2 and 4.3 ms, respectively. They were derived from the formula: $\delta = \frac{1}{2} \tan^{-1}(\pi J T_2') / (\pi J)$, where T_2' denotes either the ^{13}Cα or C′ refocused coherence lifetime (estimated to 48 and 70 ms, respectively). ^{13}Cα–^{13}C′ *J*-coupling constant of 55 Hz was assumed. ^{13}Cα evolution in t_2 (denoted t_{2B}) was performed in constant- or real-time, depending on whether t_{2B} exceeded the relaxation-optimized transfer delay δ_1 or the maximum transfer time $\delta^* = \frac{1}{2}(2J)^{-1}$. Namely, the delays δ_{3a}, δ_{3b}, δ_{3c}, δ_{3d} were set to respectively $\delta_1 - \frac{1}{2} t_{2B}$, $\frac{1}{4} t_{2B} + \frac{1}{2}(\delta_1 - pw^{CB})$, $\frac{1}{4} t_{2B} + \frac{1}{2}(\delta_1 - pw^{CB})$ and 0 if $t_{2B} < 2(\delta_1 - pw^{CB})$; to respectively pw^{CB}, $\frac{1}{2} t_{2B}$, $\frac{1}{2} t_{2B}$ and 0 if $2(\delta_1 - pw^{CB}) \le t_{2B} < 2(\delta^* - pw^{CB})$; and to respectively pw^{CB}, $\frac{1}{2} t_{2B}$, $\delta^* - pw^{CB}$ and $\frac{1}{2} t_{2B} - (\delta^* - pw^{CB})$ for $t_{2B} \ge 2(\delta^* - pw^{CB})$, where pw^{CB} stands for the duration of ^{13}Cβ-selective pulse. All pulses have phase *x* unless indicated. The phase cycle was (for convenience the numbering of phases is consistent with pulse sequence code provided below): $\phi_2 = \{y, -y\}$, $\phi_{10} = \{x, x, -x, -x\}$, $\phi_{15} = \{x, x, -x, -x\}$, $\phi_{16} = \{x, -x\}$, $\phi_{17} = y$, $\phi_{18} = x$, $\phi_{21} = x$, $\phi_{24} = x$, and $\phi_{rec} = \{y, -y, -y, y\}$. Quadrature detection in the indirect dimensions was accomplished using the States-TPPI[10] method by incrementing ϕ_2 and ϕ_{16} (in t_1) and decrementing ϕ_{10} and ϕ_{15} (in t_2), independently from t_1 and t_2 time incrementation. Additionally, a quarter spectral window upfield and downfield shift for respectively ^{15}N and ^{13}Cα resonances, was implemented by incrementing ϕ_2 and ϕ_{16} in synchrony with t_1 time incrementation, i.e. $\phi_2 = \{y, -y\} + 90° \times ((t_1\, sw_1) \bmod 4)$. The ^{15}N offset was set to 117.5 ppm while the ^{1}H offset was set on resonance with the H_2O line (approx. 4.8 ppm). The ^{13}C offset was set to the center of the ^{13}Cα band (56.4 ppm) for the first and last CP transfer, and in-between the ^{13}Cα and ^{13}C′ regions (116.4 ppm) for the rest of the sequence (as indicated by horizontal arrows). Effectively, both t_1 and t_2 ^{13}Cα evolution is performed off-resonance, and the extra acquired phase is compensated by the time-proportional phase incrementation on refocusing pulses with phases ϕ_{21} and ϕ_{24}: $\phi_{21} = \{x\} + 180 * \Delta\Omega * t_2$, $\phi_{24} = \{x\} + 180 * \Delta\Omega * t_1$ (in degrees), where $\Delta\Omega = \Omega_{C\alpha} - \Omega_0$ (in hertz). Also, all shaped ^{13}C pulses are performed off-resonance by a stepwise phase modulation with respective offset difference $\Omega_{C\alpha} - \Omega_0 = -60$ ppm, $\Omega_{C'} - \Omega_0 = 60$ ppm or $\Omega_{C\beta} - \Omega_0 = -91$ ppm (where Ω_0 stands for the carrier offset). The ^{13}C pulses for ^{15}N-^{13}Cα and ^{15}N-^{13}C′ CP transfers are performed with relative offsets $\Omega_{C\alpha} - \Omega_0 - 60$ ppm = -120 ppm and $\Omega_{C'} - \Omega_0 + 60$ ppm = +120 ppm, respectively. The additional ±60 ppm offset is to minimize undesired ^{15}N-^{13}C′ and ^{15}N-^{13}Cα transfers during these CP transfers (these lossy transfers arise due to the direction of the ^{15}N ramp enforced by other pathways). Zero phase alignment for the ^{13}C pulses during ^{15}N-^{13}Cα and ^{15}N-^{13}C′ CP transfers was enforced at the end and the beginning of the pulse, respectively. While this ensures the phase agreement for ^{13}C pulses between these two CP transfers, a constant phase difference with respect to the 90° pulse before ^{15}N-^{13}Cα CP (causing a zero-order phase for ^{13}Cα in ω_1), and with respect to the 90° pulse after ^{15}N-^{13}C′ CP is generated (leading to the loss of signal). It is thus necessary to correct these phase shifts, e.g. by empirically optimizing the phases ϕ_{16} and ϕ_{17}, while a single pathway is selected (see Section J). In our experiment, the best values of 310° and 75° were found for ϕ_{16} and ϕ_{17}, respectively. Additionally, as shown in Figure S6, among 8 recorded types of correlations there are four pairs sharing the same frequency regions in ω_1, ω_2 and ω_3 dimensions (e.g. ^{13}Cα(*i*–1)-^{15}N(*i*)-^{1}H^{N}(*i*) and ^{13}Cα(*i*)-^{15}N(*i*)-^{1}H^{N}(*i*)). They can be discriminated based on which term, i.e. either ^{15}N or ^{13}C, is present between the ^{15}N-^{13}Cα and ^{15}N-^{13}C′ CP transfers. Here, an extra 180° incrementation of phase ϕ_{18} is introduced as the innermost loop, and the interleaved data requires a linear combination (addition and subtraction) during signal processing as described in section E.

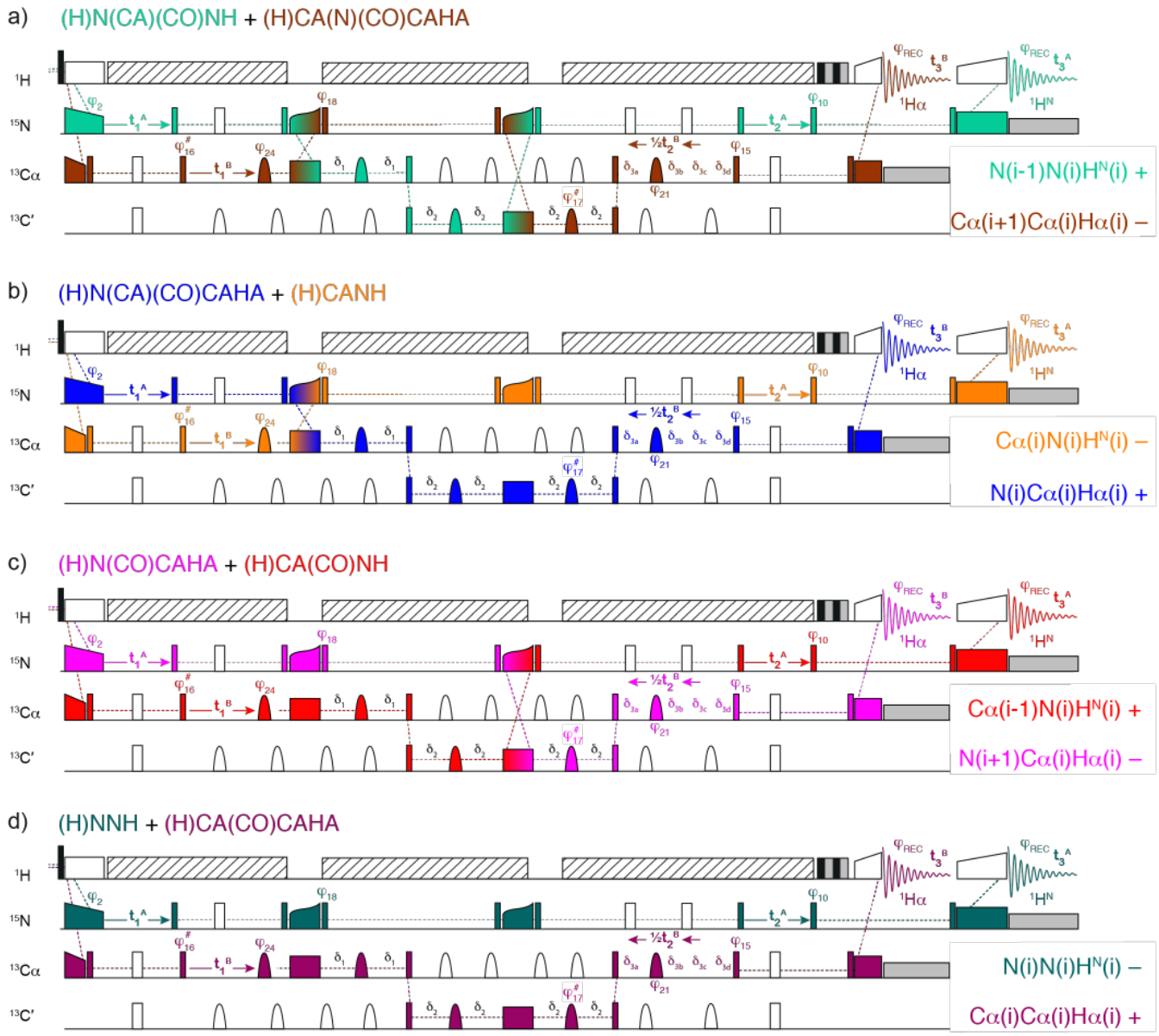

Figure S6. Scheme of 8 independent coherence transfer pathways recorded using the experiment described in Figure S5. Pathways are illustrated as dashed lines superimposed onto a simplified pulse sequence scheme from Figure S5. For clarity, the scheme was separated into 4 classes of pathways with respect to coherence response to the ^{15}N-^{13}Cα and ^{15}N-^{13}C′ CP transfers: (a) coherence transferred in both CP steps; (b) coherence transferred only in ^{15}N-^{13}Cα CP, orphan coherence utilized after ^{15}N-^{13}C′ CP; (c) orphan coherence utilized after ^{15}N-^{13}Cα CP, transferred coherence during ^{15}N-^{13}C′ CP; (d) orphan terms from both ^{15}N-^{13}Cα and ^{15}N-^{13}C′ CPs used. The types of obtained correlations are provided in bottom-right corner of each panel. "–" and "+" signs denote whether the particular correlation is observed in the "difference" or "sum" data set after a linear combination of interleaved FIDs. The "+" pathways are present as ^{13}Cα coherence just after ^{15}N-^{13}Cα CP and insensitive to ^{15}N 90° pulse phase ϕ_{18}, while "–" pathways are stored as ^{15}N coherence at this point, thus undergo a phase change according to ϕ_{18}. Direct interresidue ^{1}H^{N}-to-^{1}H^{N} and ^{1}Hα-to-^{1}Hα correlations (class "a") utilize the best possible signal, while intraresidue (class "b") and interresidue (class "c") ^{15}N-^{13}Cα-^{1}Hα and ^{13}Cα-^{15}N-^{1}H^{N} pathways make use of residual signal in one of ^{15}N-^{13}C CP. Class "d" pathways are doubly attenuated, however, these pathways are not useful for sequential assignment (byproducts).

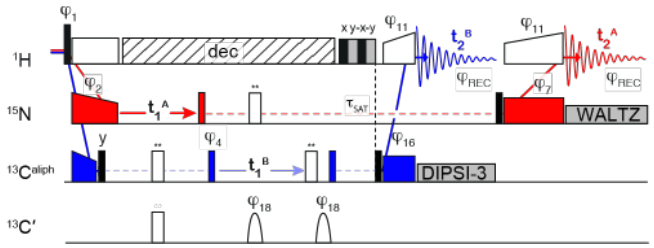

Figure S7. RF pulse scheme for the simultaneous dipolar $^{13}C,^{15}N$-HSQC experiment. The same convention for pulses and CP steps as in Figure S5 is used. RF strength, duration and detailed shapes for CP transfers are provided in Table S2. The phase cycle was: $\phi_1 = \{4(y), 4(-y)\}$, $\phi_2 = \{y, y, -y, -y\}$, $\phi_4 = \{x, x, -x, -x\}$, $\phi_7 = \{y, -y\}$, $\phi_{11} = \{8(y), 8(-y)\}$, $\phi_{16} = \{x, -x\}$, $\phi_{17} = y$, $\phi_{18} = x$, $\phi_{21} = x$, $\phi_{24} = x$, and $\phi_{rec} = \{y, -y, -y, y\}$. Quadrature detection in the indirect dimension t_1 (t_1^A for ^{15}N and t_1^B for ^{13}C) was accomplished using States-TPPI[10] method by simultaneous incrementation of ϕ_2 and ϕ_4. Offsets for ^{13}C and ^{15}N channels were set to 40.0 and 117.5 ppm, while ^1H offset was set on resonance with H_2O line (approx. 4.8 ppm). Open bell shapes on ^{13}C channels represent Q3[3] $^{13}C'$-selective pulses of 178.5 μs duration and peak RF strength of 18.49 kHz.

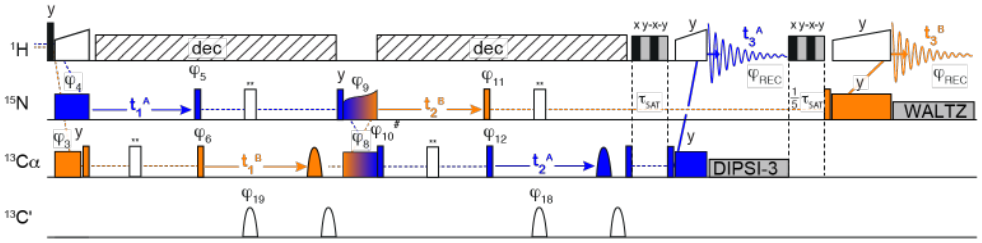

Figure S8. RF pulse scheme for the simultaneous (H)CANH and (H)NCAHA experiment ("intra-2in1"). The same convention for pulses and CP steps as in Figure S5 is used. Coherence transfer pathway is shown as dashed orange (for (H)CANH) or blue lines (for (H)NCAHA), and CP and 90° and 180° pulses are colored accordingly. RF strength, duration and detailed shapes for CP transfers are provided in Table S2. All pulses have phase x unless indicated. The phase cycle was: $\phi_3 = \{x, -x\}$, $\phi_4 = \{y, -y\}$, $\phi_5 = x$, $\phi_6 = y$, $\phi_8 = \{x, x, -x, -x\}$, $\phi_9 = \{4(x),4(-x)\}$, $\phi_{10} = y$, $\phi_{11} = y$, $\phi_{12} = x$, $\phi_{18} = \{x, y\}$, $\phi_{19} = \{x, x, y, y\}$ and $\phi_{rec} = \{2(y, -y, -y, y)\}$. The minimum phase cycle length is 4 scans. Quadrature detection in the indirect dimensions t_1 (t_1^A for ^{15}N and t_1^B for ^{13}C) and t_2 (t_2^B for ^{15}N and t_2^A for ^{13}C) was accomplished using States-TPPI[10] method by simultaneous decrementation of ϕ_5 and incrementation of ϕ_6 (in t_1) and by simultaneous decrementation of ϕ_{11} and incrementation of ϕ_{12} (in t_2). Offsets for ^{13}C and ^{15}N channels were set to 56.4 (center of $^{13}C\alpha$ region) and 117.5 ppm, while ^1H offset was set on resonance with H_2O line (approx. 4.8 ppm). Open bell shapes on ^{13}C channels represent Q3[3] $^{13}C\alpha$ and $^{13}C'$-selective pulses of durations of were 161.5 and 178.5 μs and peak RF strength of 20.43 and 18.49 kHz for $^{13}C\alpha$ and $^{13}C'$ pulses respectively. $^{13}C'$-selective pulses were performed off-resonance by phase modulation corresponding to +120 ppm with respect to ^{13}C offset. ^{13}C pulse during $^{13}C\alpha$-^{15}N CP can be performed on-resonance (with no phase modulation), however, a better selectivity of $^{15}N\rightarrow^{13}C\alpha$ transfer is achieved (for (H)NCAHA pathway) if additional –60 ^{13}C ppm offset is applied (effectively, the pulse is performed at 56.4 – 60 = –3.6 ppm). While it minimizes the competitive $^{15}N\rightarrow^{13}C'$ transfer, a constant phase difference acquired over this pulse (w.r.t. the enforced zero phase at the beginning of this pulse) must be compensated by ϕ_{20}. Empirically, in our conditions we found the best value of 325°.

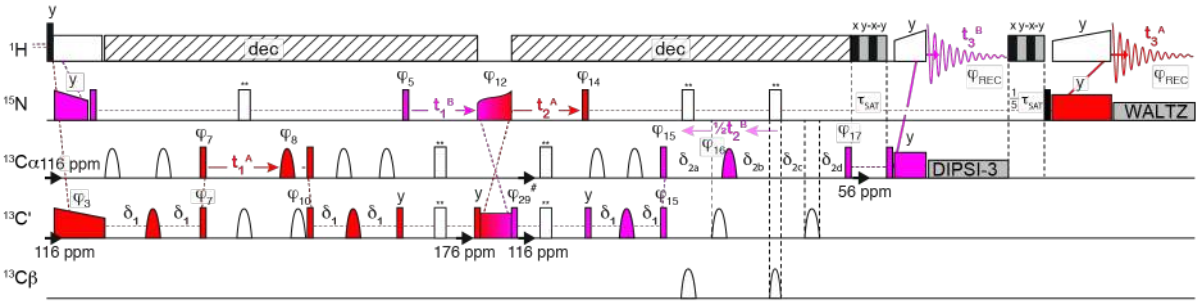

Figure S9. RF pulse scheme for the simultaneous (H)CA(CO)NH and (H)N(CO)CAHA experiment ("inter-2in1"). The same convention for pulses and CP steps as in Figure S5 is used. Coherence transfer pathway is shown as dashed red (for (H)CA(CO)NH) or magenta lines (for (H)N(CO)CAHA), and CP and 90° and 180° pulses colored accordingly. RF strength, duration and detailed shapes for CP transfers are provided in Table S2. Open bell shapes on ^{13}C channels represent Q3[3] (for ^{13}Cα and ^{13}C′) and ReBURP[4] (for ^{13}Cβ) selective pulses. Pulse durations and peak RF strength were 161.5, 178.5 and 960.9 μs and 20.43, 18.49 and 6.52 kHz for ^{13}Cα, ^{13}C′ and ^{13}Cβ pulses respectively. Relaxation-optimized ^{13}Cα–^{13}C′ *J*-transfer delays δ_1 and δ_2 were 4.3 and 4.2 ms, respectively. They were derived from the formula: $\delta = \frac{1}{2} \tan^{-1}(\pi J T_2') / (\pi J)$, where T_2' denotes either the ^{13}Cα or C′ refocused coherence lifetime (estimated to 48 and 70 ms, respectively). ^{13}Cα–^{13}C′ *J*-coupling constant of 55 Hz was assumed. ^{13}Cα evolution in t_2 (denoted t_{2B}) was performed in constant- or real-time, depending on whether t_{2B} exceeded the relaxation-optimized transfer delay δ_2 or the maximum transfer time $\delta^* = \frac{1}{2}(2J)^{-1}$. Namely, the delays δ_{2a}, δ_{2b}, δ_{2c}, δ_{2d} were set to respectively $\delta_2 - \frac{1}{2} t_{2B}$, $\frac{1}{4} t_{2B} + \frac{1}{2}(\delta_2 - pw^{CB})$, $\frac{1}{4} t_{2B} + \frac{1}{2}(\delta_2 - pw^{CB})$ and 0 if $t_{2B} < 2(\delta_2 - pw^{CB})$; to respectively pw^{CB}, $\frac{1}{2} t_{2B}$, $\frac{1}{2} t_{2B}$ and 0 if $2(\delta_2 - pw^{CB}) \le t_{2B} < 2(\delta^* - pw^{CB})$; and to respectively pw^{CB}, $\frac{1}{2} t_{2B}$, $\delta^* - pw^{CB}$ and $\frac{1}{2} t_{2B} - (\delta^* - pw^{CB})$ for $t_{2B} \ge 2(\delta^* - pw^{CB})$, where pw^{CB} stands for the duration of ^{13}Cβ-selective pulse. All pulses have phase *x* unless indicated. The phase cycle was: $\phi_3 = \{x, -x\}$, $\phi_5 = \{y, -y\}$, $\phi_7 = x$, $\phi_8 = x$, $\phi_{10} = \{x, y\}$, $\phi_{12} = \{x, x, -x, -x, -x, -x, x, x\}$, $\phi_{14} = y$, $\phi_{15} = \{x, x, -x, -x\}$, $\phi_{16} = x$, $\phi_{17} = -y$, $\phi_{29} = y$, and $\phi_{rec} = \{y, -y, -y, y, -y, y, y, -y\}$. The minimum phase cycle length is 4 scans. Quadrature detection in the indirect dimensions t_1 (t_1^A for ^{13}Cα and t_1^B for ^{15}N) and t_2 (t_2^A for ^{15}N and t_2^B for ^{13}Cα) was accomplished using States-TPPI[10] method by the simultaneous incrementation of ϕ_5 and ϕ_7 and decrementation of ϕ_3 (in t_1) and by the simultaneous decrementation of ϕ_{14} and ϕ_{17} (in t_2). ^{15}N offset was set to 117.5 ppm while ^{1}H offset was set on resonance with H_2O line (approx. 4.8 ppm). ^{13}C offset was set to in-between of ^{13}Cα and ^{13}C′ regions (116.4 ppm) for the entire experiment except the C′-^{15}N CP where it was on-resonance with C′ (176.4 ppm) and the final ^{13}Cα-^{1}Hα CP where it was at the center of ^{13}Cα band (56.4 ppm) (offset changes on the ^{13}C channel are indicated by horizontal arrows). Effectively, both t_1 and t_2 ^{13}Cα evolution is performed off-resonance, and the extra acquired phase is compensated by the time-proportional phase incrementation on refocusing pulses with phases ϕ_8 and ϕ_{16}: $\phi_8 = \{x\} - 180 * \Delta\Omega * t_1$, $\phi_{16} = \{x\} - 180 * \Delta\Omega * t_2$ (in degrees), where $\Delta\Omega = \Omega_{C\alpha} - \Omega_0$ (in hertz). Also, all shaped ^{13}C pulses are performed off-resonance by a stepwise phase modulation with respective offset difference $\Omega_{C\alpha} - \Omega_0 = -60$ ppm, $\Omega_{C'} - \Omega_0 = 60$ ppm or $\Omega_{C\beta} - \Omega_0 = -91$ ppm (where Ω_0 stands for the carrier offset at 116.4 ppm). ^{13}C pulse during ^{1}H-^{13}C′ CP is performed off-resonance with respective phase modulation, and zero phase alignment at the end of the pulse is enforced. ^{13}C pulse during ^{13}C′-^{15}N CP can be performed on-resonance (with no phase modulation), however, a better selectivity of ^{15}N→^{13}C′ transfer is achieved (for (H)N(CO)CAHA pathway) if additional ~60 ^{13}C ppm offset is applied (effectively, the pulse is performed at 176.4 + 60 = 236.4 ppm). While it minimizes the competitive ^{15}N→^{13}Cα transfer, a constant phase difference acquired over this pulse (w.r.t. the enforced zero phase at the beginning of this pulse) must be compensated by ϕ_{29}. Empirically, in our conditions we found the best value of 50°.

C. NMR data acquisition parameters

All spectra were acquired at the static field of 18.8 T (800 MHz ^{1}H). A four-channel (HCND) 0.7 mm Bruker MAS probe was used. High-power pulse durations were 2.5, 3.5 and 4.5 μs for ^{1}H, ^{13}C and ^{15}N, respectively. The sample was spun at 107 kHz, and the temperature was maintained at using a Bruker cooling unit (BCU III) with a regulated dry N_2 gas directed at the rotor. The temperature detected by the sensor (260 K) at the point where bearing, drive and VT gases are mixed, corresponds to roughly 285±5 K inside the 0.7 mm rotor. Note that in all experiments, ^{15}N and ^{13}C chemical shifts were co-evolved with time increments bound by the ration of gyromagnetic ratios: $\Delta_N = \frac{\gamma_C}{\gamma_N}\Delta_C$. Although not mandatory, this choice simplifies the immediate interpretation of chemical shifts since 1 ppm of ^{15}N and ^{13}C appear equal (e.g. ^{15}N frequencies seem scaled up if interpreted for ^{13}C evolution). The summary of acquisition parameters for multidimensional spectra of MBP can be found in Table S1.

Table S1. Acquisition parameters for multidimensional spectra acquired for the sample of U-^{13}C,^{15}N-labelled MBP.

Spectrum	Max evolution time, ms			Number of complex points			Spectral window (Hz/ppm) [a]			Scans per point	Inter-scan delay, s	Experimental time, h
	ω_1	ω_2	ω_3	t_1	t_2	t_3	ω_1	ω_2	ω_3			
(H)CH+(H)NH	37.1 (^{15}N) 15.0 (^{13}C)	24.0 (8.0)[b]		211	768 [a] (256)		5679/70.0 (^{15}N) 14085/70.0 (^{13}C)	32051/ 40.1 (^{1}H)		8	1.0	1 h
8-in-1	12.4 (^{15}N) 6.6 (^{13}Cα)	12.4 (^{15}N) 6.6 (^{13}Cα)	24.0 (8.0)[b]	106	53[c]	768 [a] (256)	6482/79.9 (^{15}N) [d] 16077/79.9 (^{13}Cα) [d]	3246/40.0 (^{15}N) 8051/40.0 (^{13}Cα)	32051/ 40.1 (^{1}H)	8 × 2[c]	0.82	118 h (4d 22h)
(H)(CA)CBCAH	6.4 (^{13}Cβ)	6.8 (^{13}Cα)	24.0 (8.0)[b]	84	44	768 [a] (256)	13089/65.0 (^{13}Cβ)	6435/32.0 (^{13}Cα)	32051/ 40.1 (^{1}H)	4	1.0	21 h
(H)(CA)CB(CA)NH	4.0 (^{13}Cβ)	10.4 (^{15}N)	20.0 (8.0)[b]	142	72	1994 (798)	17607/70 (^{13}Cβ)	3446/34 (^{15}N)	100000 /100	8	1.15	26
(H)NCAHA+ (H)CANH	23.1 (^{15}N) 9.3 (^{13}Cα)	23.1 (^{15}N) 9.3 (^{13}Cα)	24.0 (8.0)[b]	75	75	768 [a] (256)	3246/40.0 (^{15}N) 8052/40.0 (^{13}Cα)	3246/40.0 (^{15}N) 8052/40.0 (^{13}Cα)	32051/ 40.1 (^{1}H)	4	0.8	27
(H)N(CO)CAHA+ (H)CA(CO)NH	23.1 (^{15}N) 9.3 (^{13}Cα)	23.1 (^{15}N) 9.3 (^{13}Cα)	24.0 (8.0)[b]	75	75	768 [a] (256)	3246/40.0 (^{15}N) 8052/40.0 (^{13}Cα)	3246/40.0 (^{15}N) 8052/40.0 (^{13}Cα)	32051/ 40.1 (^{1}H)	8	0.8	60

[a] At the static field used (18.8 T) 1 ppm ^{1}H = 800.2 Hz, 1 ppm ^{13}C = 201.2 Hz, and 1 ppm ^{15}N = 81.1 Hz

[b] Signal truncated to ⅓ (8.0 ms) during signal processing

[c] Separation of the pathways requires an additional two-step phase-cycling on ^{15}N pulse (phase φ_{18}) as described in the caption to Figure S5. This was implemented here as an extra loop in ω_2 dimension, which thus requires a double number of complex points (106 instead of 53)

[d] Useful window is a half of the given value, since ^{15}N and ^{13}Cα resonances are shifted a quarter of spectral window upfield and downfield, respectively

Table S2. Details of cross polarization transfer

CP transfer no	Parameter	Value	Parameter name
8-in-1			
1 (^{1}H→^{15}N, ^{1}H→^{13}Cα)	contact time H–C, ms	4.0	p29
	contact time H–N, ms	4.1	p15
	^{1}H r.f. field (const), kHz	139	spw6
	^{15}N r.f. max. field, kHz	43.7	spw4
	^{13}C r.f. max. field, kHz	50.2	spw29
	^{15}N r.f. amplitude ramp[a]	67% ↓	spnam4
	^{13}C r.f. amplitude ramp[a]	75% ↓	spnam29
2 (^{15}N↔^{13}Cα)	contact time, ms	20.0	p27
	^{15}N r.f. max. field, kHz [b]	45.6	spw3
	^{15}N r.f. average field, kHz [b]	41.5	spnam3
	^{15}N r.f. modulation depth, kHz [b]	–4.1	
	^{15}N r.f. effective coupling, Hz [b]	1509	
	^{13}Cα r.f. field (const), kHz	60.0	spw9

3 ($^{13}C' \leftrightarrow ^{15}N$)	contact time, ms	18.0	p26
	$^{13}C'$ r.f. field (const), kHz	60.0	spw8
	^{15}N r.f. max. field, kHz [b]	43.7	spw2
	^{15}N r.f. average field, kHz [b]	39.8	spnam2
	^{15}N r.f. modulation depth, kHz [b]	–4.0	
	^{15}N r.f. effective coupling, Hz [b]	1447	
4 ($^{1}H \leftarrow ^{13}C\alpha$)	contact time, ms	0.2	p30
	^{13}C r.f. field (const), kHz	28.0	spw30
	^{1}H r.f. max. field, kHz	139	spw7
	^{1}H r.f. amplitude ramp [a]	20% ↑	spnam7
4' ($^{1}H \leftarrow ^{15}N$)	contact time, ms	0.9	p17
	^{15}N r.f. field (const), kHz	27.9	spw5
	^{1}H r.f. max. field, kHz	139	spw10
	^{1}H r.f. amplitude ramp [a]	20% ↑	spnam10
$^{13}C,^{15}N$-HSQC			
1 ($^{1}H \rightarrow ^{15}N$, $^{1}H \rightarrow ^{13}C\alpha$)	contact time H–C, ms	0.5	p29
	contact time H–N, ms	1.0	p15
	^{1}H r.f. field (const), kHz	159	spw6
	^{15}N r.f. max. field, kHz	45.4	spw2
	^{13}C r.f. max. field, kHz	68.9	spw29
	^{15}N r.f. amplitude ramp [a]	54% ↓	spnam2
	^{13}C r.f. amplitude ramp [a]	54% ↓	spnam28
2 ($^{1}H \leftarrow ^{13}C\alpha$)	contact time, ms	0.2	p30
	^{13}C r.f. field (const), kHz	26.8	spw30
	^{1}H r.f. max. field, kHz	153	spw7
	^{1}H r.f. amplitude ramp [a]	20% ↑	spnam7
2' ($^{1}H \leftarrow ^{15}N$)	contact time, ms	0.9	p17
	^{15}N r.f. field (const), kHz	25.6	spw20
	^{1}H r.f. max. field, kHz	151	spw10
	^{1}H r.f. amplitude ramp [a]	20% ↑	spnam10
SIM-(H)CANH,(H)NCAHA			
1 ($^{1}H \rightarrow ^{15}N$, $^{1}H \rightarrow ^{13}C\alpha$)	contact time H–C, ms	1.09	p29
	contact time H–N, ms	1.1	p15
	^{1}H r.f. max. field, kHz	141	spw6
	^{15}N r.f. max. field (const), kHz	27.5	spw2
	^{13}C r.f. max. field (const), kHz	26.8	spw29
	^{1}H r.f. amplitude ramp [a]	20% ↓	spnam6
2 ($^{15}N \leftrightarrow ^{13}C\alpha$)	contact time, ms	20.0	p16
	^{15}N r.f. max. field, kHz [b]	44.8	spw3
	^{15}N r.f. average field, kHz [b]	40.7	spnam3
	^{15}N r.f. modulation depth, kHz [b]	–4.1	
	^{15}N r.f. effective coupling, Hz [b]	1482	
	$^{13}C\alpha$ r.f. field (const), kHz	60.0	spw9
3 ($^{1}H \leftarrow ^{13}C\alpha$)	contact time, ms	0.2	p30
	^{13}C r.f. field (const), kHz	26.8	spw30
	^{1}H r.f. max. field, kHz	153	spw7
	^{1}H r.f. amplitude ramp [a]	20% ↑	spnam7

3' (^{1}H←^{15}N)	contact time, ms	0.9	p17
	^{15}N r.f. field (const), kHz	27.5	spw20
	^{1}H r.f. max. field, kHz	150.6	spw10
	^{1}H r.f. amplitude ramp [a]	20% ↑	spnam10
SIM-(H)CA(CO)NH,(H)N(CO)CAHA			
1 (^{1}H→^{15}N, ^{1}H→^{13}C′)	contact time H–C, ms	6.5	p28
	contact time H–N, ms	3.3	p15
	^{1}H r.f. field (const), kHz	139	spw6
	^{15}N r.f. max. field, kHz	38.6	spw2
	^{13}C r.f. max. field, kHz	36.9	spw28
	^{15}N r.f. amplitude ramp [a]	67% ↓	spnam2
	^{13}C r.f. amplitude ramp [a]	75% ↓	spnam28
2 (^{13}C′↔^{15}N)	contact time, ms	20.0	p16
	^{13}C' r.f. field (const), kHz	60.9	spw8
	^{15}N r.f. max. field, kHz [b]	46.2	spw3
	^{15}N r.f. average field, kHz [b]	42.0	spnam3
	^{15}N r.f. modulation depth, kHz [b]	–4.2	
	^{15}N r.f. effective coupling, Hz [b]	1530	
3 (^{1}H←^{13}Cα)	contact time, ms	0.2	p30
	^{13}C r.f. field (const), kHz	28.4	spw30
	^{1}H r.f. max. field, kHz	158	spw7
	^{1}H r.f. amplitude ramp [a]	20% ↑	spnam7
3' (^{1}H←^{15}N)	contact time, ms	0.9	p17
	^{15}N r.f. field (const), kHz	28.0	spw20
	^{1}H r.f. max. field, kHz	152	spw10
	^{1}H r.f. amplitude ramp [a]	20% ↑	spnam10

[a] An x % ramp means a linear amplitude modulation from (1-x/100) to 1.0 (ramp "up" ↑), or from 1.0 to (1-x/100) ("ramp down" ↓)

[b] The tangential shapes (for adiabatic CP[11]) are defined by 4 empirical parameters: the average RF field ω_{avg} (close to the Hartmann-Hahn matching condition), the effective dipolar coupling d^{eff} (averaged over crystal orientations and decreased due to internal motions), the modulation depth Δ, and the contact time τ, according to the following equation:

$$\omega(t) = \omega_{avg} + d^{eff} \tan\left(\frac{2}{\tau}\operatorname{atan}\left(\frac{\Delta}{d^{eff}_{NC}}\right)\left(\frac{\tau}{2} - t\right)\right)$$

Negative modulation depth thus corresponds to a decreasing RF field strength during CP.

D. Sensitivity of RAVASSA pathways

The two primary experiments in RAVASSA approach, which provide direct connectivities between neighboring residues (dubbed NNH and CCH) utilize the optimal coherence transfer pathway. They are only affected by a slight interference of the first cross-polarization, which is quantified in Figure S3 (approximate losses are 6 and 16% for H–C and H–N transfers, respectively). In contrast, the other 6 pathways rely on the orphan (untransferred) signal after one or two C–N cross-polarizations, and are thus inevitably weaker than independently optimized single-spectra. Our rough estimations based on unresolved 1D spectra show 30-40% relative efficiency of the relevant pathways, and larger attenuation of two redundant sub-spectra (3D analogues of (H)NH and (H)CH experiments). However, decreased efficiency of the relevant 4 pathways is, to a large extent, compensated by their higher intrinsic sensitivity. As a result, the intensity of RAVASSA subspectra is better balanced than reference (independent) experiments leading to better allocation of measurement time, as shown in Figure S10. Table S3 compares the integrals of 1D signal of all experiments presented in this work to a suite of conventional (serially acquired) ones.

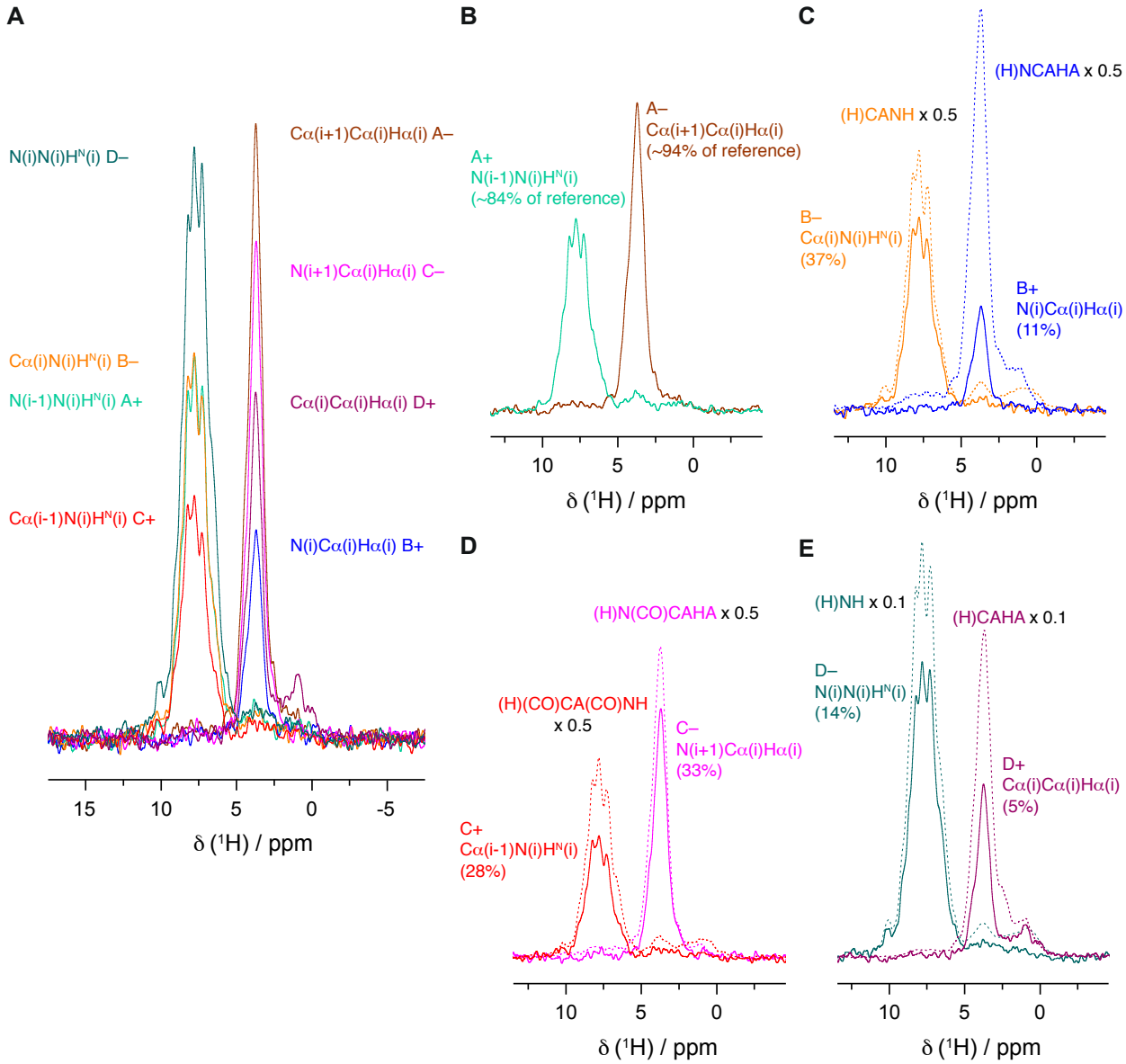

Figure S10. Relative intensities of eight RAVASSA pathways as observed in ^{1}H 1D first-FID spectra (A), color-coded and labeled "A+", "A–" etc. in agreement with pathway description in respective panels A, B, etc. of Figure S6. Selection of pathways was performed using appropriate phase cycling as described in Section J. Note that due to lack of resolution and line width differences, the intensity comparison is valid only between $^{1}H^{N}$- or $^{1}H\alpha$-detected pathways. Panels B-E show the 1D intensity comparisons of RAVASSA pathways (divided into four classes as in Figure S6) with the corresponding separately optimized serial experiments (dashed curves). Relative integral of respective 1D signals is given for every pathway.

Table S3. Summary of sensitivity of simultaneously and serially acquired experiments on MBP

$^1H^N$-detected [a]				$^1H\alpha$-detected [b]			
Experiment	Mode	Relative sensitivity, [c] %		Experiment	Mode [c]	Relative sensitivity, [c] %	
(H)NH	conv. [d]	100 [e]	100	(H)CH (Cα-sel.)	conv. [d, n]	100 [e]	100
	2-in-1 [f]	81	81		2-in-1 [f]	92	92
	8-in-1 [g, h]	14	14		8-in-1 [g, h]	4.5	4.5
(H)CANH	conv. [d]	23	100	(H)NCAHA	conv. [d]	25	100
	2-in-1 [i]	21	87		2-in-1 [i]	19	76
	8-in-1 [g]	8.7	37		8-in-1 [g, o]	2.8	11
(H)CONH	conv. [d]	33	–	(H)COCAHA	conv. [d]	34	–
(H)(CO)CA(CO)NH	conv. [d]	19	100	(H)N(CO)CAHA	conv. [d]	20	100
	2-in-1 [j]	19	99		2-in-1 [j]	17	85
	8-in-1 [g, k]	5.4	28		8-in-1 [g]	6.6	33
(H)CO(CA)NH	conv. [d]	8.8	–	(H)CO(N)CAHA	conv. [d]	17	–
(H)(CA)CB(CA)NH	conv. [d]	8.1 [l]	–	(H)(CA)CBCAHA	conv. [d]	27 [l]	–
(H)(CA)CB(CA)(CO)NH	conv. [d]	8.8 [l]	–	(H)CA(N)(CO)CAHA	8-in-1 [g]	8.4	94 [m]
(H)N(CA)(CO)NH	8-in-1 [g]	8.4	84 [m]				

[a] The table reports on sensitivity estimated as an integral of backbone amide ^1H signal between 11 and 5 ppm in 1D 1st FID experiments (64 scans, 8 ms signal truncation, and the exponential line broadening of 100 Hz).

[b] Similarly, but alpha ^1H signal was integrated between 6 and 2.5 ppm in 1D 1st FID experiments.

[c] The left column reports on sensitivity with respect to either (H)NH or (H)CH-Cα-selective experiment, while the values in the right column refer to the respective conventional (serially acquired) experiment in each case.

[d] An independently optimised conventional (serially acquired) experiment.

[e] The value of the signal integral was $1.2 \cdot 10^9$ for (H)NH, as compared to $1.17 \cdot 10^9$ for Cα-selective (H)CH experiment (in arbitrary units).

[f] The SIM-^{13}C,^{15}N-CP-HSQC experiments described in Figure S7.

[g] The 8-in-1 (RAVASSA) experiment described in Figures S5 and S6

[h] In the 8-in-1 data set these pathways result in 3D diagonal correlations, affecting S/N by an additional factor of √2 w.r.t. 2D spectra

[i] The SIM-(H)CANH,(H)NCAHA experiment described in Figure S8.

[j] The SIM-(H)(CO)CA(CO)NH,(H)N(CO)CAHA experiment described in Figure S9.

[k] In the 8-in-1 data set these correlations originate from (H)CA(CO)NH pathway

[l] In these experiments the signal transferred from $^{13}C\alpha$ to $^{13}C\beta$ partially cancels with residual untransferred one, and with this of glycine-$^{13}C\alpha$. The relative sensitivity measured in 1D mode is thus underestimated.

[m] The corresponding conventional experiments were not acquired. The estimation is based on the performance of first CP (see caption to Figure S3).

[n] The (H)CH experiment with an additional $^{13}C\alpha$-selective refocusing pulse in t_1

[o] In the 8-in-1 acquisition mode these correlation originate from the less sensitive (H)N(CA)(CO)CAHA pathway.

E. NMR data processing

nmrPipe processing (8-in-1 data set)

In the first step data is imported and separated into four folders HAc, HAn, HNc, HNn, depending on the detected nucleus and signal response to phase ϕ_{18} (code Listing 2). Next, Fourier transformation and usual data manipulation (apodization, phasing, zero filling) is performed (code Listing 3). Finally, ω_1 dimension is split to generate spectra with either $^{13}C\alpha$ or ^{15}N shifts in ω_1, and (optionally) converted to UCSF format. Note that resulting spectra need the adjustment of carrier frequency, offset (in ppm), and sweep widths after splitting of ω_1 dimension if ^{15}N chemical shifts are evolved instead of ^{13}C. This was performed using `ucsfdata` utility from Sparky package.

Listing 2. Data import to nmrPipe format and separation of spectra by addition/subtraction

```
#!/bin/csh

bruk2pipe -in ./ser \
  -bad 0.0 -aswap -DMX -decim 624 -dspfvs 20 -grpdly 67.9911956787109  \
  -xN              1536  -yN               424  -zN               212  \
  -xT               768  -yT               212  -zT               106  \
  -xMODE            DQD  -yMODE        Complex  -zMODE        Complex  \
  -xSW        32051.282  -ySW         8051.530  -zSW        16077.171  \
  -xOBS         800.150  -yOBS         201.198  -zOBS         201.198  \
  -xCAR           4.800  -yCAR          56.700  -zCAR          56.700  \
  -xLAB             HNx  -yLAB             13C  -zLAB             13Cz  \
  -ndim               3  -aq2D          States                         \
  -out ./fid/test%03d.fid -verb -ov

 xyz2pipe -in fid/test%03d.fid -x -verb \
| nmrPipe -fn QMIX -ic 4 -oc 1 -time -cList \
  1,0  \
  0,0  \
  1,0  \
  0,0  \
| pipe2xyz -out HAc/test%03d.fid -verb -ov

 xyz2pipe -in fid/test%03d.fid -x -verb \
| nmrPipe -fn QMIX -ic 4 -oc 1 -time -cList \
  1,0  \
  0,0  \
 -1,0  \
  0,0  \
| pipe2xyz -out HAn/test%03d.fid -verb -ov

 xyz2pipe -in fid/test%03d.fid -x -verb \
| nmrPipe -fn QMIX -ic 4 -oc 1 -time -cList \
  0,0  \
  1,0  \
  0,0  \
  1,0  \
| pipe2xyz -out HNc/test%03d.fid -verb -ov

 xyz2pipe -in fid/test%03d.fid -x -verb \
| nmrPipe -fn QMIX -ic 4 -oc 1 -time -cList \
  0,0  \
  1,0  \
  0,0  \
 -1,0  \
| pipe2xyz -out HNn/test%03d.fid -verb -ov
```

Listing 3. nmrPipe Fourier processing

```
#!/bin/csh

xyz2pipe -in fid/test%03d.fid -x -verb \
| nmrPipe  -fn EXT -xn 256 -sw \
| nmrPipe  -fn SP -off 0.33 -end 1.0 -pow 2 -c 0.5  \
| nmrPipe  -fn ZF -size 2048                        \
| nmrPipe  -fn FT                                   \
| nmrPipe  -fn EXT -x1 {$1}ppm -xn {$2}ppm -sw -verb  \
| nmrPipe  -fn PS -p0 -95.200 -p1 0.0 -di            \
| nmrPipe  -fn TP                                   \
| nmrPipe  -fn SP -off 0.33 -end 1.0 -pow 2 -c 0.5 \
| nmrPipe  -fn ZF -size 256                         \
| nmrPipe  -fn FT -alt                              \
| nmrPipe  -fn PS -p0 0.0 -p1 0.0 -di               \
| pipe2xyz -out ft/test%03d.ft2 -y

xyz2pipe -in ft/test%03d.ft2 -z -verb                \
| nmrPipe  -fn SP -off 0.33 -end 1.0 -pow 2 -c 0.5   \
| nmrPipe  -fn ZF -size 256                          \
| nmrPipe  -fn FT -alt                             \
| nmrPipe  -fn PS -p0 0.0 -p1 0.0 -di                \
| pipe2xyz -out ft/test%03d.ft3 -z
```

```
# EXT -left selects 13CA pathway in t1 (z)
xyz2pipe   -in ft/test%03d.ft3 -z -verb           \
| nmrPipe  -fn EXT -left  -sw -verb               \
| pipe2xyz -out F1c/test%03d.ft3 -z

# EXT -right  selects 15N pathway in t1 (z)
xyz2pipe -in ft/test%03d.ft3 -z -verb              \
| nmrPipe  -fn EXT -right  -sw -verb               \
| pipe2xyz -out F1n/test%03d.ft3 -z
```

F. Joint manual analysis of intra and interresidue H^N and Hα-detected spectra

We present in Figure S11 a scheme for manual data analysis of reduced 8-in-1 data set comprising only intra- and interresidue ^{1}Hα- and $^1H^N$-detected ^{15}N-^{13}Cα-^{1}H correlations (4 spectra). In particular, we envisage its utility for the cases of limited sample sensitivity, where the NNH and CCH pathways might not yield sufficient signals for a significant fraction of residues.

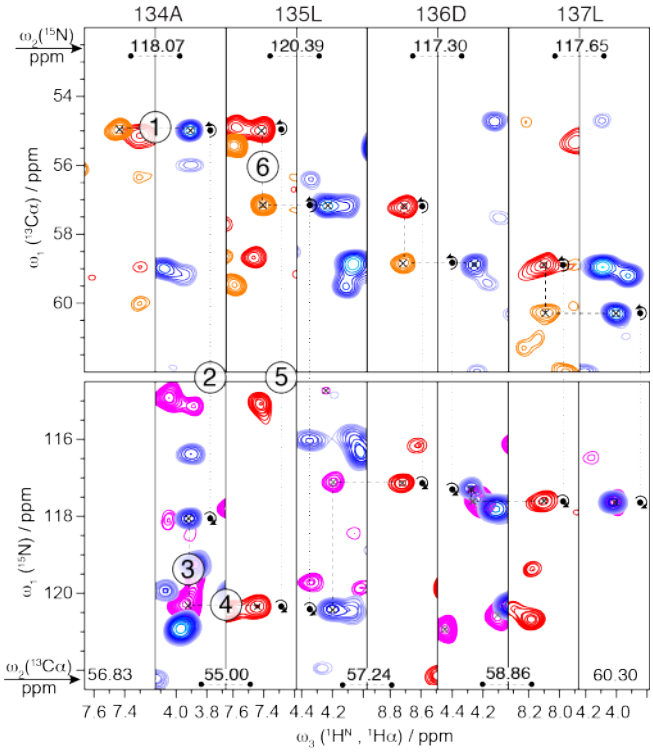

Figure S11. Strategy for sequential assignment of backbone resonances based on intra- (*orange* and *blue* contours) and interresidue correlations (*red* and *magenta* contours) recorded simultaneously in $^1H^N$-detected (*odd* strips counting from left-to-right) and ^{1}Hα-detected (*even* strips) experiments: (H)NCAHA (*blue*), (H)N(CO)CAHA (*pink*), (H)CANH (*red*), (H)CA(CO)NH (*orange* contours). Representative ω_1(either ^{13}Cα or ^{15}N)-ω_3(^{1}H) cross-sections of 3D spectra of MBP (for residues 134-137) are shown at the ω_2 (either ^{15}N or ^{13}Cα) frequency indicated in each strip. Key steps 1, 3, 4, and 6 of the process connect peaks which share two frequencies and lead to one new chemical shift, thus avoid the ambiguity encountered with conventional stripplots. Steps "2" and "5" represent 3D-rotations of spectra (around the peak indicated with a curling arrow) which allow to alternate between ^{13}Cα–^{1}H (*top*) and ^{15}N–^{1}H (*bottom*) planes.

G. Details of automated assignment

Below we provide the batch script for CYANA program used to invoke FLYA assignment routine for MBP data (Listing S4). The outcome is summarized in Tables S4 and S5, which report on completeness of resonance assignment with respect to nuclei types and particular peak lists. Additionally, Table S6 provides evidence on the synergy between datasets comprising RAVASSA. Finally, Figure S12 illustrates the extent of assignment divided by *pathway* (either direct amide-to-amide (NNH), alpha-to-alpha (CCH), ^{15}N-linking with ^{1}Hα-detection or ^{1}Hα-linking with $^1H^N$-detection).

Listing 4. FLYA batch script

```
structurepeaks:=
assignpeaks:=CACAHA,hCAcoNH,hCANH,hNCAHA,hNcoCAHA,NNH,CBCAHA,CBcaNH

#tolerances for FLYA
assigncs_accH:=0.1
assigncs_accC:=0.3
assigncs_accN:=0.3

#these tolerances are not used for FLYA
tolerance:=0.1,0.1,0.3

shiftassign_population:=50
shiftassign_iterations:=15000

randomseed  := 3771

command select_atoms
  atom select "N H  HA HA2 HA3 CA CB"
end

analyzeassign_group:= BB: N H HA HA2 HA3 CA CB, ALL:*

read lib ../../ssFLYA_1H_detected.pro.lib append
read seq mbp.seq

flya runs=20 assignpeaks=$assignpeaks structure=
```

Table S4. FLYA resonance assignment summary

Nucleus	Max	FLYA [a]	
			%
$^{1}H^{N}$	349 [b]	285	82
^{15}N	341 [c]	293	86
	21 [d]	11	52
	371	304	82
$^{1}H\alpha$	371 [e]	307	83
	384-393 [f]	318 [f]	81-83
	401 [g]	318	79
$^{13}C\alpha$	371	314	85
$^{13}C\beta$	341	272	80
ALL	1803 [h]	1482	82

[a] Strongly assigned resonances, i.e. above and internal FLYA threshold of 0.8

[b] The number of amide protons, i.e. excluding proline residues and N-terminus

[c] excluding proline ^{15}N atoms

[d] proline ^{15}N atoms only

[e] diastereotopic $^{1}H\alpha_2$ and $^{1}H\alpha_3$ atoms of 30 glycine residues treated as one entity, irrespective of their chemical shift difference

[f] counting diastereotopic $^{1}H\alpha_2$ and $^{1}H\alpha_3$ glycine atoms as different if assigned chemical shifts differ by at least 0.05 ppm. The maximum number of shifts is estimated based on the strongly assigned ("known") diastereotopic shifts, indistinguishable within ^{1}H linewidth (the case of 8 glycine residues)

[g] assuming that all diastereotopic $^{1}H\alpha_2$ and $^{1}H\alpha_3$ atoms of 30 glycine residues are distinguishable (upper limit for the number of shifts)

[h] given the conditions [b] and [e] above (all backbone ^{15}N spins, but consolidated $^{1}H\alpha_2$ and $^{1}H\alpha_3$ glycine shifts)

Table S5. Summary of peak lists used for automated assignment

Spectrum	Number (and percentage) of peaks		
	Expected [a]	Measured [b]	Assigned [c]
(H)N(CA)(CO)NH	349	275 (79%)	258 (94%)
(H)CA(N)(CO)CAHA	400 / 370	308 (77%)	268 (87%)
(H)CANH	349	302 (87%)	266 (88%)
(H)N(CA)(CO)CAHA	401 / 371	309 (77%)	201 (65%)
(H)CA(CO)NH	349	294 (84%)	248 (84%)
(H)N(CO)CAHA	400 / 370	282 (70%)	266 (94%)
(H)(CA)CB(CA)NH	320	243 (76%)	228 (94%)
(H)(CA)CBCAH	341	316 (93%)	284 (89%)
ALL	2909	2329 (80%)	2019 (87%)

[a] The maximum number of peaks expected from allowed magnetization pathways. For Hα-detected experiments upper and lower limits are given, depending on the feasibility to resolve correlations of diastereotopic glycine $^{1}H\alpha_2$ and $^{1}H\alpha_3$ spins

[b] The peaks identified in spectra and the percentage w. r. t. the number of expected peaks. Note that due to limited spectral resolution, and near-equivalent $^{1}H\alpha_2$ and $^{1}H\alpha_3$ shifts of glycine residues, some expected peaks, although detectable, may remain unresolved in the experiment (the percentage is underestimated)

[c] The number of measured peaks which were assigned and the percentage given w. r. t. all measured peaks

Table S6. FLYA resonance assignment summary with partial data inputs

Nucleus	Max	CCH+NNH+CB [a]	%	All – CCH – NNH [b]	%	Union of sets [c]	%	RAVASSA excess [d]	%
$^{1}H^{N}$	349 [e]	29	8	94	27	103	30	182	52
^{15}N	371 [f]	32	9	98	26	108	29	196	53
$^{1}H\alpha$	371 [g]	39	11	112	30	134	36	173	47
$^{13}C\alpha$	371	47	13	112	30	128	35	186	50
$^{13}C\beta$	341	40	12	92	27	110	32	162	48
ALL	1803 [h]	187	10	508	28	583	32	899	49

[a-d] The number of resonances strongly assigned by FLYA

[a] The input reduced to (H)CA(N)(CO)CAHA, (H)N(CA)(CO)NH, (H)(CA)CB(CA)NH and (H)(CA)CBCAH peak lists

[b] The input reduced to (H)CANH, (H)CA(CO)NH, (H)CA(N)(CO)CAHA, (H)N(CO)CAHA, (H)(CA)CB(CA)NH and (H)(CA)CBCAH peak lists

[c] Resonance counts for the union of resonance sets of previous columns ([a] and [b])

[d] The synergy effect of a full RAVASSA dataset: a difference of resonance count between these given in Table S4 and the union of 2 sets for partial data input

[e] The number of amide protons, i.e. excluding proline residues and N-terminus

[f] proline ^{15}N atoms inclusive

[g] diastereotopic $^{1}H\alpha_2$ and $^{1}H\alpha_3$ atoms of 30 glycine residues treated as one entity, irrespective of their chemical shift difference

[h] given the conditions [b] and [e] above (all backbone ^{15}N spins, but consolidated $^{1}H\alpha_2$ and $^{1}H\alpha_3$ glycine shifts)

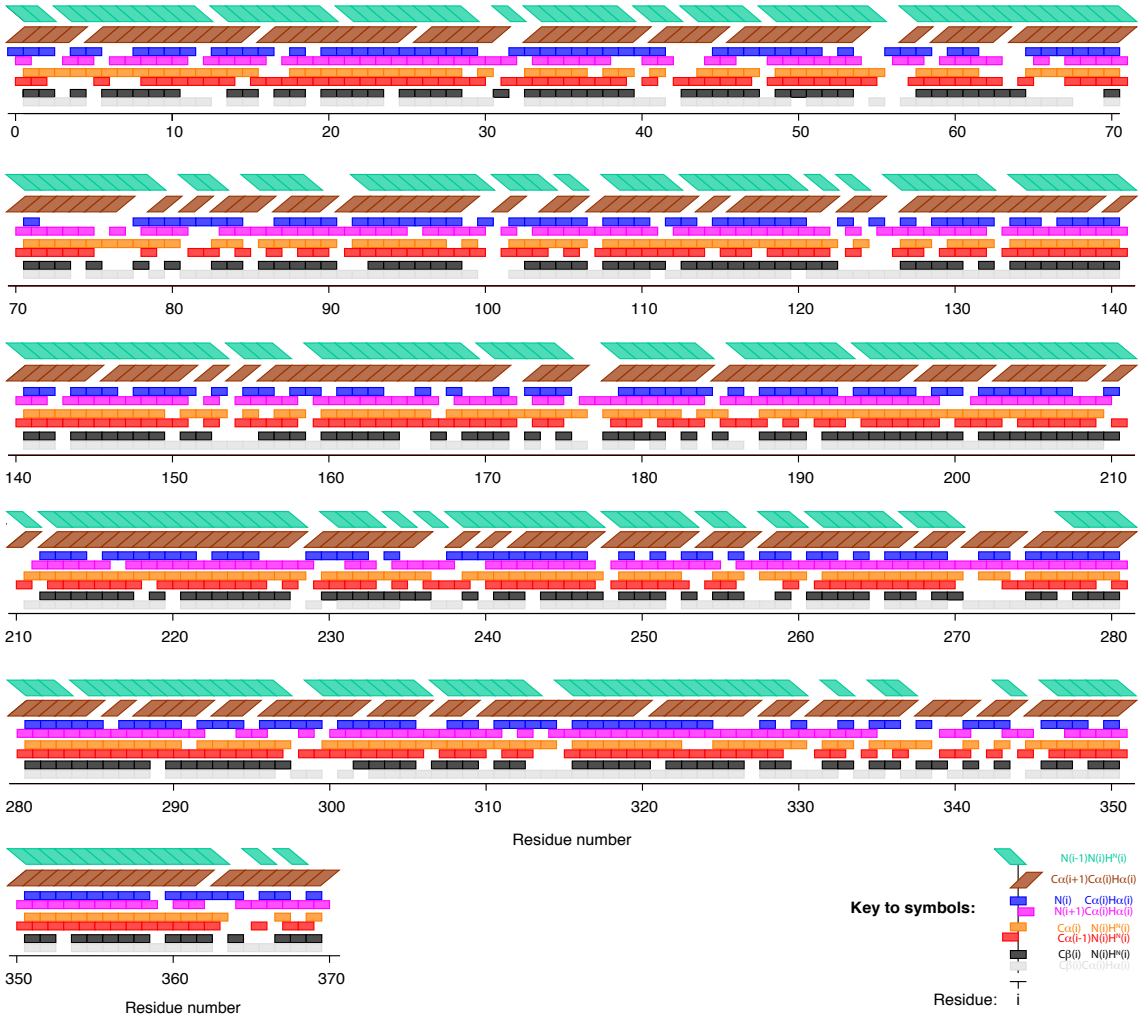

Figure S12. Extent of FLYA assignment of observed 3D resonance correlations in 6 simultaneously recorded RAVASSA subspectra and two intraresidue ^{13}Cβ correlations. The four pathways which allow (in principle independent) linking between resonances in neighboring residues are shown as boxes with the following color-coding, from top to bottom of each panel: *light green* (N(*i*–1)–N(*i*)–HN(*i*)); *brown* (Cα(*i*+1)–Cα(*i*)–Hα(*i*)); *blue* (N(*i*)–Cα(*i*)–Hα(*i*)) and *magenta* (N(*i*+1)–Cα(*i*)–Hα(*i*)); *orange* (Cα(*i*)–N(*i*)–H^N(*i*)) and *red* (Cα(*i–1*)–N(*i*)–H^N(*i*)). Additionally, assigned ^{13}Cβ–N(*i*)–H^N(*i*) and ^{13}Cβ–Cα(*i*)–Hα(*i*) correlations are shown in dark and light grey, respectively.

H. Chemical shifts of MBP in the solid-state versus in solution

The resonance chemical shifts obtained with FLYA were compared to those of maltotriose-bound MBP (in the "closed" conformation) studied in solution by Kay and co-workers[12] (BMRB entry no 4987). This is the closest match among available BMRB depositions for this protein, taking the kind of ligand as a primary criterion. Since the protein in solution required extensive deuteration, ^{13}Cα and ^{13}Cβ shifts required a correction of ^{2}H isotope effect (using standard formulae of Venters and co-workers[13]) before a comparison to ^{13}C, ^{15}N-labelled MBP used in our study. Based on these shifts we first prepared a synthetic 2D ^{13}C-^{13}C correlation, assuming uniform intensities and resonance line widths (94 and 59 Hz for ^{13}Cβ and ^{13}Cα respectively). Figure S13a shows its superposition (*black* contours) with a 2D ω_1- ω_2 projection of 3D (H)(CA)CBCAHA spectrum in the solid-state (*red* contours) restricted to regions of ^{13}Cβ–^{13}Cα correlations. Positions of majority of peaks agree very well between precipitated and solute MBP, and a presence of a few minor differences is in line with analogous comparisons on GB1[14] and other model proteins. In contrast, the superposition of a synthetic ^{15}N-HSQC (solution) and experimental CP-^{15}N-HSQC (solids) in panel *b* of Figure S13 shows significant differences for amide ^{15}N and ^{1}H shifts. They arise most likely due to crystal ^{1}H-^{1}H contacts, different patterns of hydrogen bonds between the two sample formulations, conformational averaging in solution, and generally larger susceptibility of amide ^{1}H and ^{15}N (when compared to ^{13}C) shifts to the chemical environment, e.g. buffer pH (7.2 in solution vs. 8.0 in solids), ionic strength, the presence of precipitant etc.

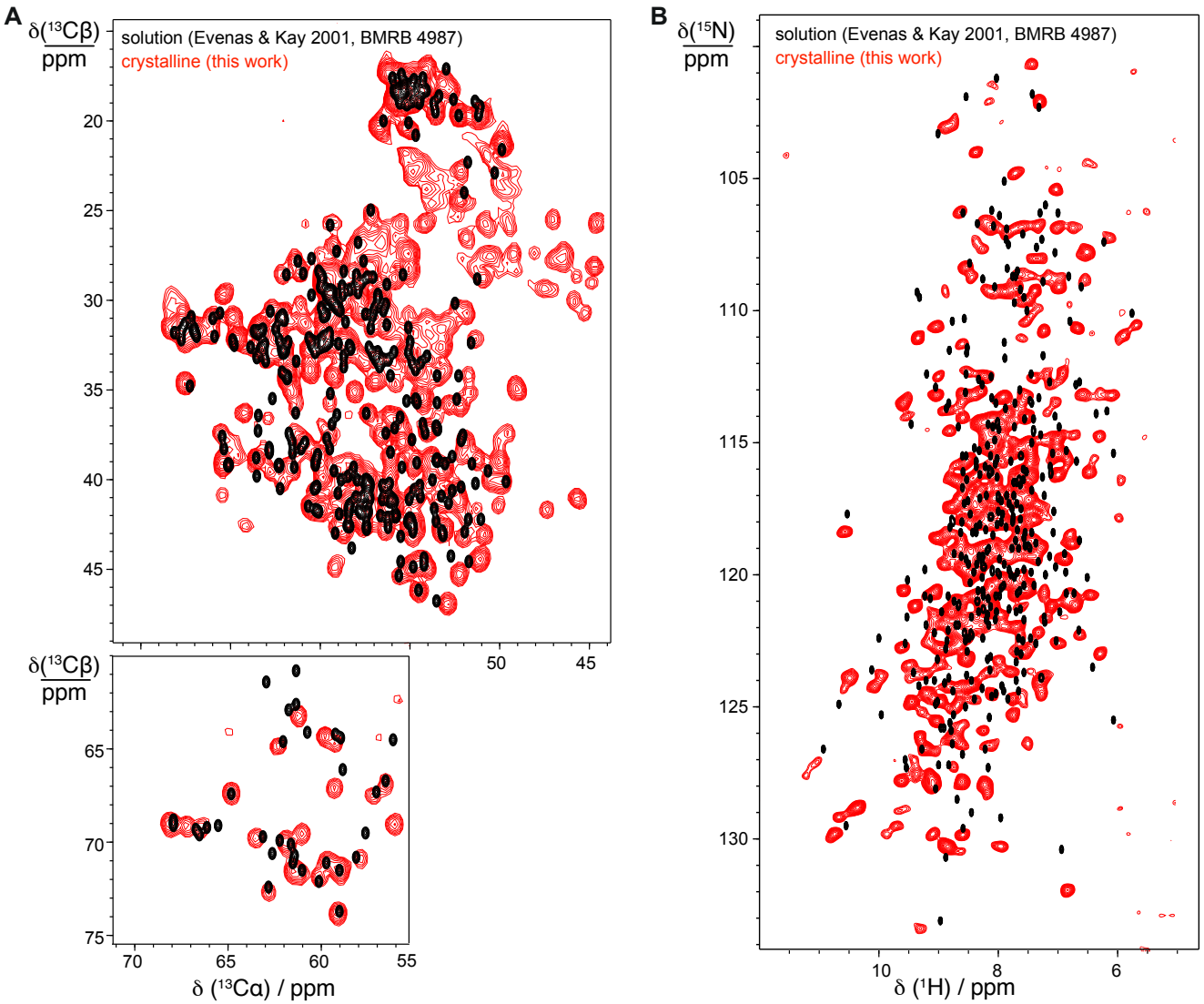

Figure S13. (A) Superposition of 2D ^{13}Cβ–^{13}Cα regions of ^{13}C–^{13}C correlation spectrum of maltotriose-bound MBP in solution (*black* contours, synthetic – based on shifts in BMRB entry no 4987) and in the crystalline preparation (*red* contours). (B) Comparison of a synthetic ^{15}N-HSQC (solution, in black) and experimental CP-^{15}N-HSQC (solids, in red).

I. Extensions of the FLYA library

Below we provide the FLYA definitions of correlations observed in eight simultaneous experiments used in this study, and two additional ones which provide intraresidue ^{13}Cβ correlations. Note that definitions 3-6 below are also suitable to describe peaks in SIM-(H)CANH,(H)NCAHA and SIM-(H)(CO)CA(CO)NH,(H)N(CO)CAHA experiments.

1. **(H)N(CA)(CO)NH**, correlation N(i–1) – N(i) – H^N (i)

```
SPECTRUM sshNcacoNH N2 N1 H1
0.980  N2:N_AMI C_ALI C_BYL N1:N_AMI H1:H_AMI
```

Note that this definition allows the pathway origin at proline ^{15}N, which are usually only weakly polarized with H–N CP. It also permits the pathways starting at N-terminal ^{15}N-spins.

2. **(H)CA(N)(CO)CAHA**, correlation Cα (i+1) – Cα (i) – Hα (i)

```
SPECTRUM ssCAncoCAHA C2 C1 H1
0.980  C2:C_ALI (C_BYL) N_AMI C_BYL C1:C_ALI (N_AMI) H1:H_ALI
```

3. **(H)CANH**, correlation Cα (i) – N(i) – H^N (i)

```
SPECTRUM sshCANH  HN N C
0.980  HN:H_AMI N:N_AMI (C_BYL) C:C_ALI
```

4. **(H)N(CA)(CO)CAHA**, correlation N (*i*) – Cα (*i*) – Hα (*i*)

```
SPECTRUM sshNcacoCAHA  N C HC
0.980  N:N_AMI C:C_ALI (C_BYL) HC:H_ALI
```

Note that this definition allows the pathway origin at proline ^{15}N but excludes detection at Lys/His/Arg side-chain amide/amine protons (to distinguish from (H)NCAH experiment where such peaks can in principle be observed).

5. **(H)CA(CO)NH**, correlation Cα (*i*–1) – N(*i*) – H^N (*i*)

```
SPECTRUM ssCAcoNH HN N C
0.98   HN:H_AMI N:N_AMI (C_ALI) C_BYL C:C_ALI
```

Note that this definition discards side-chain Asn/Gln peaks.

6. **(H)N(CO)CAHA**, correlation N (*i*+1) – Cα (*i*) – Hα (*i*)

```
SPECTRUM sshNcoCAHA  N C HC
0.980  N:N_AMI (C_ALI) C_BYL C:C_ALI HC:H_ALI
```

Note that this definition discards side-chain Asn/Gln peaks, but allows proline ^{15}N as the origin of the pathway.

7. **(H)NNH**, "diagonal" correlation N(*i*) – N(*i*) – H^N (*i*)

```
SPECTRUM sshNNH  N11 N1 H1
0.980  N11:N1:N_AMI (C_BYL) (C_ALI) H1:H_AMI
```

8. **(H)CA(CO)CAHA**, "diagonal" correlation Cα (*i*) – Cα (*i*) – Hα (*i*)

```
SPECTRUM sshCAcoCAHA  C11 C1 H1
0.980  C11:C1:C_ALI (C_BYL) (N_AMI) H1:H_ALI
```

9. **(H)(CA)CB(CA)NH**, correlation Cβ (*i*) – N(*i*) – H^N (*i*)

```
SPECTRUM ssCBcaNH  HN N C
0.980  HN:H_AMI  N:N_AMI (C_BYL) C_ALI C:C_ALI
```

Note that the N-terminal residue is excluded. Glycine residues, which give Cα (*i*) – N(*i*) – H^N (*i*) signals of opposite signs, are not considered either.

10. **(H)(CA)CBCAHA**, correlation Cβ (*i*) – Cα (*i*) – Hα (*i*)

```
SPECTRUM ssCBCAHA  HA CA CB
0.980  HA:H_ALI CA:C_ALI (N_AMI) (C_BYL) CB:C_ALI
```

J. Pulse programs in Bruker code

Note that all pulse programs provided below require two memory buffers (NBL=2) to store separate Hα and H^N signals (in a single scan). This enforces an additional pseudo-dimension (innermost, either F2 or F3) with TD=2, thus experiments are acquired as 3D instead of 2D, and 4Ds instead of 3Ds. All programs support the disabling of inversion pulses on either ^{15}N or ^{13}Cα channel during ^{13}Cα or ^{15}N chemical shift evolution, respectively, via –DNOINVPUL flag in ZGOPNTS, or non-zero counter l3 (for code Listing 8). The co-evolution of ^{15}N and ^{13}C is governed by constant 21 (cnst21), which standard value is 2.4803 (a ratio of ^{13}C and ^{15}N gyromagnetic ratios). In the particular case of 8-in-1 experiment (Listing 8), additional counters l1, l2 and l4 are provided to allow selection of specific pathway. In such test (either 1D or 2D) experiments, a phase cycle on phase ϕ_{18} should be disabled using –DNOSEPARATION flag. Instead of multiplexing with phase ϕ_{18}, L2 counter allows to observe only (+) pathways (l2=0) *or* (–) pathways (l2=2) (refer to caption to Figure S6 for details). L1 counter determines whether Hα signal only (l1=0), Hα and H^N (l1=1), or H^N signal only (l1=2) is stored. Finally, counter L4 allows to select pathways regarding the magnetization behavior during ^{13}C-^{15}N CP, and correspond to pathways shown in Figure S6a (l4=2), S6b (l4=3), S6c (l4=4), S6d (l4=5) or all of them (l4=1).

Listing 5. Bruker pulse program for SIM-^{13}C,^{15}N-CP-HSQC

```
; 1H-detected cp experiment
;with 15N and 13C decoupling
;written by kurt zilm
;modified for simultaneous acquisition by jan stanek

;Avance II+ version
;parameters:
;p1 : 1H 90 pulse @ plw1
```

```
;pl1 : 1H power for 90 pulse

;p15 : contact time for H->N CP
;sp2 : 15N power for H->N CP
;sp6 : 1H power for H->N CP

;p17 : contact time for N->H CP
;sp20 : 15N power for N->H CP
;sp10 : 1H power for N->H CP
;spnam10 : e.g. Ramp100.90
;spoffs10 : 0

;p7 : 15N 90 pulse @ plw7
;pl7 : 15N power for 90 pulse

;p3 : 13C 90 pulse @ plw3
;pl3 : 13C power for 90 pulse

;cpdprg1 : 1H decoupling (sltppm_40pTr41 for 1Hprot)
;cpdprg2 : 15N decoupling (waltz16_pl16)
;cpdprg3 : 13C decoupling (dipsi3_pl17)

;pl13: 1H decoupling (sltppm)
;pl16: 15N decoupling power (waltz16)
;pl17: 13C decoupling power (dipsi3)

;pcpd2 : 25u (waltz16 10 kHz)
;pcpd3 : 12.5u (dipsi3 20 kHz)


;$COMMENT=basic cp experiment, arbitrary contact and decoupling schemes
;$CLASS=Solids
;$DIM=1D
;$TYPE=cross polarisation
;$SUBTYPE=simple 1D
;$OWNER=Bruker
prosol relations=<solids_cp>

#include <Avancesolids.incl>

;cnst11 : to adjust t=0 for acquisition, if digmod = baseopt
;"acqt0=1u*cnst11"
"in0=inf1"

; 1H settings
"spoal6=0"
"spoff6=0"
"spoal7=0"
"spoff7=0"
"spoff10=0"
"spoal10=0"

; 15N settings
"plw16=plw7*(pow(p7/25,2))"     ; 15N waltz 10kHz decoupling power level
"spoal2=0"
"spoff2=0"
"spoal20=0"
"spoff20=0"

; 13C settings
"plw11=plw3"
"plw17=plw3*(pow(p3/12.5,2))"     ; 13C DIPSI-3 20kHz decoupling power level
"spoal29=0"
"spoff29=0"
"spoff30=0"
"spoal30=0"

"cnst24 = (sfo3-bf3)*1000000/bf3"  ; C aliph frequency offset (ppm)
"cnst20 = cnst24-(42.7-173.3)"     ; CO frequency offset (ppm)

"p18=3.412/(95.0*bf3/1000000)"    ; 95 ppm bandwidth (safe)
"spw18=plw3*pow((0.5/(p18*0.1515))/(0.25/p3),2)" ;  Q3 power level
"spoal18=0.5"                      ; default value (irrelevant)
"spoff18=bf3*((cnst20-cnst24)/1000000)"                       ; CO on resonance
```

```
;cnst21 : = tmax(15N)/tmax(13C), may not be larger than 5 to avoid folding 15N dimension!
;2.4803
"d15=d0*cnst21"
"in15=in0*cnst21"

;l1 : 1 (both HA and HN), 0 (only HA), 2 (only HN) signal recorded

"d3=trunc((p1+de)*cnst31/1000000+0.9999)*(1s/cnst31)-p1/1000000"
"d4=d3-de"

; store HN and HA in the independent FIDs (change a memory buffer)
if "nbl == 2" goto NOERROR

print "error: Please reserve space for separate FIDs with NBL=2"
goto HaltAcqu

NOERROR, 1u

1 ze
2 d1 do:f2 do:f3
#include <p15_prot.incl>
#include <aq_prot.incl>

1m st0

 (p1 ph1 pl1):f1

 (1u p29:sp29 ph3 1u pl11 p3 ph21):f3 (1u p15:sp2 ph2):f2 (p15:sp6 ph10 1u cpds1):f1

; 15N co-evolution
#ifdef NOINVPUL
  d15
  (p7 pl7 ph5):f2
#else
  if "d15 >= p3*4" {
    (center (d15) (p3 ph0 pl11 p3*2 ph20 pl11 p3 ph0 pl11):f3)
    (p7 pl7 ph5):f2
  } else {
       d15
       (p7 pl7 ph5):f2
       ; always do at least one 13C 180 pulse
       1u
       (p3 ph0 pl11 p3*2 ph20 pl11 p3 ph0 pl11):f3
  }
#endif

  10u
  ; flip-down 13C
  5m

 (p3 pl11 ph4):f3
  d0*0.5
  4u
#ifdef NOINVPUL
  (p18:sp18 ph18):f3
#else
  (center (p18:sp18 ph18):f3 (p7 ph0 pl7 p7*2 ph20 pl7 p7 ph0 pl7):f2)
#endif
  4u
  d0*0.5
  (p3 pl11 ph9 p3*2 pl11 ph0 p3 pl11 ph9):f3
  4u
  (p18:sp18 ph0):f3
  4u
  (p3 pl11 ph6):f3  (1u do):f1

;;;;;;;;;;;;;;;; water suppression block starts
 1u pl12:f1
 (d30*0.25 cw ph12):f1
 (d30*0.25 cw ph13):f1
 (d30*0.25 cw ph14):f1
 (d30*0.25 cw ph15):f1
 1u do:f1
```

```
;;;;;;;;;;;;;;;; water suppression block ends
if (l1 != 2)
{
  (p3 ph8 pl11):f3
  (p30:sp30 ph16):f3 (p30:sp7 ph11):f1
  d3
  (p1*2 pl1 ph0):f1
  d4
}
if (l1 == 0) {; collect only HA signal
  go=2   ph31 cpds3:f3 finally do:f3
}
if (l1 == 1) {
  goscnp ph31 cpds3:f3 finally do:f3
}

1m st

if (l1 != 0)
{
  (p7 ph8 pl7):f2
  (p17:sp20 ph7):f2 (p17:sp10 ph11):f1
  d3
  (p1*2 pl1 ph0):f1
  d4
  go=2 ph31 cpds2:f2 finally do:f2
}

  10m mc #0 to 2
  F1PH(calph(ph2,+90) & calph(ph4,+90), caldel(d15,+in15) & caldel(d0,+in0))
  F2QF()              ; a fake loop (td2 should always be 2, corresponding to NBL=2)

HaltAcqu, 1m  ;jump address for protection files
exit                                      ;quit

ph0 = 0
ph1 = {1}*4 {3}*4
ph2 = 1 1 3 3
ph3 = 0
ph4 = 0 0 2 2
ph5 = 0
ph6 = 0
ph7 = 1 3
ph8 = 0
ph9 = 1
ph10 = 0
ph11 = {1}*8 {3}*8
ph12 = 0
ph13 = 1
ph14 = 2
ph15 = 3
ph16 = 3 1
ph20 = 1
ph21 = 1
ph18 = 0 1
ph31 = 1 3 3 1 3 1 1 3
       3 1 1 3 1 3 3 1
```

Listing 6. Bruker pulse program for SIM-(H)CANH,(H)NCAHA

```
;Avance II+ version
;parameters:
;pl3 : 13C power
;pl13 : 1H decoupling power level
;d1 : recycle delay
;sp3 : CN CP
;pcpd1 : pulse length for 1H decoupling sequence
;pcpd2 : pulse length for 15N dec during acq (25.0 us)
;pcpd3 : pulse length for 13C dec during acq (12.5 us)
;zgoptns : -Dlacq, -DNOINVPUL or blank
```

```
;$COMMENT=basic cp experiment, arbitrary contact and decoupling schemes
;$CLASS=Solids
;$DIM=3D
;$TYPE=cross polarisation
;$SUBTYPE=simple 1D
;$OWNER=CRMN
prosol relations=<solids_cp>

#include <Avancesolids.incl>

;cnst11 : to adjust t=0 for acquisition, if digmod = baseopt

; 1H settings
"spoal6=0"
"spoal7=0"
"spoff6=0"
"spoff7=0"

; 15N settings
"plw2=plw7"
"plw16=plw2*(pow(p7/25,2))"        ; 15N waltz 10kHz decoupling power level
"spoal3=0.5"                       ; default value (irrelevant)
"spoff3=0.0"                       ; on-resonance

"spoal2=0.5"                        ; default value (irrelevant)
"spoff2=0"                         ; N on resonance
"spoal20=0.5"                      ; default value (irrelevant)
"spoff20=0"                        ; N on resonance

; 13C settings
"plw11=plw3"

"plw17=plw3*(pow(p3/12.5,2))"     ; 13C dipsi3 20kHz decoupling power level

"cnst22 = (sfo3-bf3)*1000000/bf3"  ; CA frequency offset (ppm)
"cnst24 = cnst22+(173.7-53.7)"     ; CO frequency offset (ppm)

"p18=3.412/(95.0*bf3/1000000)"    ; 95 ppm bandwidth (safe)
"spw18=plw3*pow((0.5/(p18*0.1515))/(0.25/p3),2)" ;  Q3 power level
"spoal18=0.5"                      ; default value (irrelevant)
"spoff18=bf3*((cnst24-cnst22)/1000000)"

"p19=3.412/(105.0*bf3/1000000)"      ; 95 ppm bandwidth (safe)
"spw19=plw3*pow((0.5/(p19*0.1515))/(0.25/p3),2)" ;  Q3 power level
"spoal19=0.5"                       ; default value (irrelevant)
"spoff19=0.0"                       ; CA frequency (on-resonance)

;spoffs9 : set to 0 for on-resonance N-CA CP, or ~-60 ppm off-resonance (regulate PHCOR10 then!)
"spoff29=0.0"                       ; on-resonance CA
"spoff30=0.0"                       ; on-resonance CA
"spoal9=0"                         ; phase aligned to 0 at the end (if off-resonance)
"spoal29=0"
"spoal30=0"

"acqt0=1u*cnst11"

"in0=inf1"
"in10=inf2"

;cnst21 : = tmax(15N)/tmax(13C), may not be larger than 5 to avoid folding 15N dimension!
; a value of 2.4803 gives correct ranges (but not the offset) in ppm

"d0=0"
"d10=0"
"d15=d0*cnst21"
"in15=in0*cnst21"
"d16=d10*cnst21"
"in16=in10*cnst21"

"d3=p17-p30-p3-1u"
"p14=p16-1u-p3"
"d7=p7"

aqseq 321
```

```
1 ze
2 d1 do:f2 do:f3

#include <p15_prot.incl>
#include <aq_prot.incl>

1m st0

  (p1  pl1 ph1):f1
  (p29:sp29 ph3 1u pl11 p3 ph1):f3 (p15:sp2 ph4):f2 (p15:sp6 ph2):f1
  1u cpds1:f1

  ; 15N co-evolution
  if "d15 >= p3*4" {
       (center (d15) (p3 ph0 pl11 p3*2 ph20 pl11 p3 ph0 pl11):f3)
       (p7 pl7 ph5):f2
} else {
    d15
    (p7 pl7 ph5):f2
       ; always do at least one 13C 180 pulse
    (p3   ph0  pl11 p3*2 ph20 pl11 p3   ph0  pl11):f3
  }
  10u

  ; flip-down 13C
  (p3 pl11 ph6):f3
  d7
  d0*0.5
  4u
#ifdef NOINVPUL
  (p18:sp18 ph19):f3 ;CO decoupling pulse
#else
  (center (p18:sp18 ph19):f3 (p7 ph0 pl7 p7*2 ph20 pl7 p7 ph0 pl7):f2)
#endif
  d0*0.5
  4u
  (p19:sp19 ph0):f3 ;CA selective pulse
  4u
  (p18:sp18 ph0):f3 ;CO decoupling pulse
  4u
  (p7 ph7 pl7):f2 (1u do):f1 ; flip-down 15N

  (p14:sp9 ph8 1u p3 ph10:r pl11):f3 (p16:sp3 ph9):f2  ; CP 13C<->15N (bidirectional)

;
; the second combined 15N/13C editing
;

1u cpds1:f1

#ifdef NOINVPUL
  d16
  (p7 pl7 ph11):f2
#else
  if "d16 >= p3*4" {
       (center (d16) (p3 ph0 pl11 p3*2 ph20 pl11 p3 ph0 pl11):f3)
       (p7 pl7 ph11):f2
  } else {
    d16
       (p7 pl7 ph11):f2
       1u
    ; always do at least one 13C 180 pulse
       (p3 ph0 pl11 p3*2 ph20 pl11 p3 ph0 pl11):f3
  }
#endif

  10u

  ; flip-down 13C
  (p3 pl11 ph12):f3
  d10*0.5
  4u
#ifdef NOINVPUL
```

```
  (p18:sp18 ph18):f3 ;CO decoupling pulse
#else
  (center (p18:sp18 ph18):f3 (p7 ph0 pl7 p7*2 ph20 pl7 p7 ph0 pl7):f2)
#endif
  4u
  d10*0.5
  (p19:sp19 ph0):f3 ;CA selective pulse
  4u
  (p18:sp18 ph0):f3 ;CO decoupling pulse
  4u
  (p3 pl11 ph13):f3  (1u do):f1 ; 13CA flip-up

; solvent suppression
  1u pl12:f1
  (d30*0.25 cw ph21):f1
  (d30*0.25 cw ph22):f1
  (d30*0.25 cw ph23):f1
  (d30*0.25 cw ph24):f1
  1u do:f1
;;;;;;;;;;;;;;;; water suppression block ends
; collect 13CA->1HA signal
  (p3 pl11 ph14):f3
  (p30:sp30 ph15):f3 (p30:sp7 ph16):f1
  goscnp ph31 cpds3:f3 finally do:f3

  1m st
  1u pl12:f1
  (d30*0.05 cw ph21):f1
  (d30*0.05 cw ph22):f1
  (d30*0.05 cw ph23):f1
  (d30*0.05 cw ph24):f1
  1u do:f1

  ; collect 15N->1HN signal
  (p7 pl7 ph14):f2
  (p17:sp20 ph15):f2 (p17:sp10 ph16):f1
  go=2 ph31 cpds2:f2 finally do:f2

;  1u cpds2:f2 cpds3:f3
 ; go=2 ph31
;  1m do:f2    do:f3
  10m mc #0 to 2
  F3QF()                              ; a fake loop (td3 should always be 2, corresponding to NBL=2)
  F1PH(calph(ph5, -90) & calph(ph6, +90),  caldel(d0,  +in0)  & caldel(d15, +in15))
  F2PH(calph(ph11, -90) & calph(ph12, +90), caldel(d10, +in10) & caldel(d16, +in16))

HaltAcqu, 1m  ; jump address for protection files
exit

ph0  = 0
ph1  = 1
ph2  = 0
ph3  = 0 2
ph4  = 1 3
ph5  = 0
ph6  = 1
ph7  = 1
ph8  = 0 0 2 2
ph9  = 0 0 0 0 2 2 2 2
ph10 = 1
ph11 = 1
ph12 = 0
ph13 = 0
ph14 = 0
ph15 = 1
ph16 = 1
ph18 = 0 1
ph19 = 0 0 1 1
ph20 = 1
ph21 = 0
ph22 = 1
ph23 = 2
ph24 = 3
ph31 = 1 3 3 1 3 1 1 3
```

Listing 7. Bruker pulse program for SIM-(H)(CO)CA(CO)NH,(H)N(CO)CAHA

```
;Avance II+ version
;parameters:
;p1 : 13C 90 pulse for 180 in t1
;pl3 : 13C power for 180
;p3 : proton 90 at power level pl12
;p15 : contact time at pl1 (f1) and pl2 (f2)
;pl1 : X power level during contact
;sp0 : proton power level during contact
;pl2 : =120dB, not used
;pl12 : decoupling power level (if not pl13)
;pl13 : special decoupliong power level
;d1 : recycle delay
;cnst21 : ratio for 15N sampling
;pcpd2 : pulse length in decoupling sequence
;pcpd4 : pulse length for X dec during acq
;cpdprg2 : cw, tppm (at pl12), or lgs, cwlg. cwlgs (LG-decoupling
;spnam0 : use e.g. ramp.100 for variable amplitude CP
;here pl13 is used instead of pl12)
;zgoptns : -Dfslg, -Dlacq, or blank

;$COMMENT=basic cp experiment, arbitrary contact and decoupling schemes
;$CLASS=Solids
;$DIM=1D
;$TYPE=cross polarisation
;$SUBTYPE=simple 1D
;$OWNER=Bruker
prosol relations=<solids_cp>

#include <Avancesolids.incl>

; 1H settings
"spoal6=0.5"    ; default value (irrelevant)
"spoff6=0.0"    ; on-resonance
"spoal7=0.5"   ; default value (irrelevant)
"spoff7=0.0"   ; on-resonance
"spoal10=0.5"   ; default value (irrelevant)
"spoff10=0.0"   ; on-resonance

; 15N settings
"spoal2=0.5"                      ; default value (irrelevant)
"spoff2=0"                         ; CA on resonance
"spoal20=0.5"                      ; default value (irrelevant)
"spoff20=0"                         ; CA on resonance

"plw2=plw7"
"plw16=plw2*(pow(p7/25,2))"     ; 15N waltz 10kHz decoupling power level
"spoal3=0.5"   ; default value (irrelevant)
"spoff3=0.0"     ; on-resonance

; 13C settings
"plw11=plw3"
"plw17=plw3*(pow(p3/12.5,2))"     ; 13C dipsi 20kHz decoupling power level

"cnst22 = (sfo3-bf3)*1000000/bf3"  ; CA frequency offset (ppm)
"cnst19 = cnst22+(173.3-53.3)"     ; CO frequency offset (ppm)
"cnst23 = cnst22+(113.3-53.3)"     ; the offset half-way CO and CA (ppm)
"cnst20 = cnst22-(53.3-22.3)"     ; special CB frequency offset (ppm)

; States-TPPI phase increment for CA off-resonance evolution (offset shift emulation)
"cnst24 = -360*(cnst22-cnst23)*bf3/2" ; CA TPPI phase increment (t1), with States-TPPI
"cnst25 = -360*(cnst22-cnst23)*bf3/2" ; CA TPPI phase increment (t2), with States-TPPI

              ;"/2" because it is to be applied for 180 pulse

"p18=3.412/(95.0*bf3/1000000)"    ; 95 ppm bandwidth (safe)
"spw18=plw3*pow((0.5/(p18*0.1515))/(0.25/p3),2)" ;  Q3 power level
"spoal18=0.5"                      ; default value (irrelevant)
"spoff18=bf3*((cnst19-cnst23)/1000000)" ;  CO frequency (offset CO/CA)

"p19=3.412/(105.0*bf3/1000000)"      ; 95 ppm bandwidth (safe)
"spw19=plw3*pow((0.5/(p19*0.1515))/(0.25/p3),2)" ;  Q3 power level
```

```
"spoal19=0.5"                              ; default value (irrelevant)
"spoff19=bf3*((cnst22-cnst23)/1000000)"   ; CA frequency (offset CO/CA)

"p22=4.64/(24*bf3/1000000)" ; CB: 24 ppm bandwidth (25+12=37 ppm band;no effect from 25+18=43 ppm)
"spw22=plw3*pow((0.5/(p22*0.0798))/(0.25/p3),2)" ;  ReBURP power level
"spoal22=0.5"                         ; default value (irrelevant)
"spoff22=bf3*((cnst20-cnst23)/1000000)" ; CB offset from CO/CA

"spoal28=1"
"spoff28=bf3*((cnst19-cnst23)/1000000)" ; CO offset on CA/CO

"spoff30=0"
  ; on-resonance CA
"spoal30=0.5"

;"spoff8=0"
  ; on-resonance CO, NO: NOW IT IS RELEASED TO ALLOW OFF-RESONANCE CP
  ;BUT IN THIS CASE, PHASE 29 HAS TO BE CORRECTED EMPIRICALLY (PHCOR29 != 0)
;"spoal8=0.5"
"spoal8=0"
;by convention now, (H)(CO)CA(CO)NH pathway is unperturbed, (H)N(CO)CAHA pathway requires PHCOR29
"p14=p16-2*p3-1u"

; transfer delays
"d11=0.5*atan(cnst11*PI*55.0)/(PI*55)"    ; J(CO-CA)=55, relax. CO optimized delay
"d12=0.5*atan(cnst10*PI*55.0)/(PI*55)"    ; J(CO-CA)=55, relax. CA optimized delay
"d5=0.25/55"

aqseq 321

;cnst21 : = tmax(15N)/tmax(13C), may not be larger than 5 to avoid folding 15N dimension!
;2.4803
; Start evolutions exactly from 0
"d0=0"
"d10=0"

"d15=d0*cnst21"
"d16=d10*cnst21"

"in0=inf1"
"in10=inf2"

"d4=p3*2/3.14"
"d19=p16-2u"
"d7=4*p7"
"d20=d12-p22"
"d3=d5-p22"

"d13=larger(0,d20-d10*0.5)"
"d14=larger(d10*0.5,d10*0.25+d20*0.5)"
"d17=-larger(-d14,-d3)"
"d18=larger(0,d10*0.5-d3)"

1 ze
2 d1 do:f2 do:f3
#include <p15_prot.incl>
#include <aq_prot.incl>

1m st0

  "d13=larger(0,d20-d10*0.5)"
  "d14=larger(d10*0.5,d10*0.25+d20*0.5)"
  "d17=-larger(-d14,-d3)"
  "d18=larger(0,d10*0.5-d3)"

  ; 15N evolution periods
  "d15=d0*cnst21"
  "d16=d10*cnst21"

  10u
  "cnst27=cnst24*d0" ; phase shift CA t1 (TPPI)
  10u
  "cnst26=cnst25*d10" ; phase shift CA t2 (TPPI)
  10u ip8+cnst27
```

```
  10u ip16+cnst26

  1u fq=cnst23 (bf ppm):f3  ; offset in between of CO/CA

  (p1 ph1 pl1):f1
  (p28:sp28 ph3):f3 (p15:sp2 ph4 1u pl7 p7 ph0):f2 (p28:sp6 ph2):f1

  1u cpds1:f1
  4u
  (p19:sp19 ph0):f3 ; CA selective pi pulse

  d11
  d4
  (p18:sp18 ph0):f3 ; CO selective pi pulse
  5u
  (p19:sp19 ph0):f3 ; CA selective pi pulse
  d11

  (p3 pl11 ph7):f3  ; CO&CA pi/2 pulse

  4u
  d0*0.5
#ifdef NOINVPUL
  (p18:sp18 ph0):f3
#else
  (center (p18:sp18 ph0):f3 (p7 pl7 ph26 p7*2 pl7 ph0 p7 pl7 ph26):f2)  ;CO selective Pi and 15N
  180
#endif
  d0*0.5
  4u
  (p19:sp19 ph8):f3  ;CA selective Pi
  4u
  (p18:sp18 ph10):f3 ; CO selective pi pulse
  4u

  (p3 ph9 pl11):f3   ; pulse CA / CO

  d11
  (p19:sp19 ph0):f3
  4u
  (p18:sp18 ph0):f3
  d11
  (p19:sp19 ph0):f3

  4u
  (p3 ph21 pl11):f3

  1m ; zz-filter for elimination of undesired coherences

  1u fq=cnst19 (bf ppm):f3  ; offset CO

; 15N evolution (t1) part
#ifndef NOINVPUL
  1u
  if "d15 < 4*p3" {
       (p3 ph0 p3*2 ph24 p3 ph0):f3
  }
  1u

  (p7 ph5 pl7):f2

  if "d15 >= 4*p3" {
    (center (d15) (p3 ph0 p3*2 ph24 p3 ph0):f3)
  } else {
       d15
  }
  1u fq=cnst19 (bf ppm):f3  ; offset CO
#else
  1u fq=cnst19 (bf ppm):f3  ; offset CO
  (p7 ph5 pl7):f2
  d15
#endif

  ;;;;;;;;;;; CP 13C<->15N (bidirectional, CO on resonance) ;;;;;;;;;;;;;;;;
```

```
  ; flip-down CO at the beginning of CP
  ; flip-back CO at the end of CP
  ; 13C offset in between of CO/CA at the end of 13CO-15N CP

  (p3 pl11 ph22 p14:sp8 ph11 p3 pl11 ph29 1u fq=cnst23 (bf ppm)):f3    (p16:sp3  ph12):f2  (1u  do
  d19 1u cpds1):f1


;;;;;;;;;;;;;;;;;;;;;;;;;;;;;;;;;;;;;;;;;;;;;;;;;;;;;;;;;;;;;;;;;;;;;;;;;;;

  ; 15N (t2) evolution
#ifdef NOINVPUL
  d16
  (p7 pl7 ph14):f2
#else
  if "d16 >= 4*p3" {
    (center (d16) (p3 ph0 p3*2 ph24 p3 ph0):f3)
  } else {
       d16
  }
  (p7 pl7 ph14):f2
  if "d16 < 4*p3" {
       (p3 ph0 p3*2 ph24 p3 ph0):f3
  }
#endif

  ; 13C z-filter
  1m

  ; flip-down CO (offset is CA/CO)
  (p3 ph23 pl11):f3
  4u
  (p19:sp19 ph0):f3 ; CA selective pulse
  d11
  (p18:sp18 ph0):f3 ; CO selective pulse
  4u
  (p19:sp19 ph0):f3 ; CA selective pulse
  d11

  (p3 ph15 pl11):f3 ; pulse CA / CO

  d13*0.5
#ifndef NOINVPUL
  (center (p22:sp22 ph30):f3 (p7 pl7 ph26 p7*2 pl7 ph0 p7 pl7 ph26):f2); CB selective Pi (reburp)
  and 15N 180 pulse
#else
  (p22:sp22 ph30):f3  ; just CB selective Pi (reburp)
#endif
  d13*0.5

  (p18:sp18 ph0):f3  ; CO selective pulse
  4u
  (p19:sp19 ph16):f3 ; CA (and CB) pulse
  d14

#ifndef NOINVPUL
  (center (p22:sp22 ph30):f3 (p7 pl7 ph26 p7*2 pl7 ph0 p7 pl7 ph26):f2); CB selective Pi (reburp)
  and 15N 180 pulse
#else
  (p22:sp22 ph30):f3  ; just CB selective Pi (reburp)
#endif

  d17
  (p18:sp18 ph0):f3  ; CO selective pulse (Bloch-Siegert phase)
  d18
  4u

(p3 ph17 pl11):f3 (1u do):f1 ; pulse CA / CO

  1u fq=cnst22 (bf ppm):f3  ; offset CA

; solvent suppression
  1u pl12:f1
  (d30*0.25 cw ph25):f1
```

```
  (d30*0.25 cw ph26):f1
  (d30*0.25 cw ph27):f1
  (d30*0.25 cw ph28):f1
  1u do:f1
  ;;;;;;;;;;;;;;;; water suppression block ends
  ; collect 13CA->1HA signal
  (p3 pl11 ph18):f3
  (p30:sp30 ph19):f3 (p30:sp7 ph20):f1
  goscnp ph31 cpds3:f3 finally do:f3

 1m st
 1u pl12:f1
  (d30*0.05 cw ph25):f1
  (d30*0.05 cw ph26):f1
  (d30*0.05 cw ph27):f1
  (d30*0.05 cw ph28):f1
  1u do:f1

  ; collect 15N->1HN signal
  (p7 pl7 ph18):f2
  (p17:sp20 ph19):f2 (p17:sp10 ph20):f1
  go=2 ph31 cpds2:f2 finally do:f2


10m mc #0 to 2
  F3QF()
  F2PH(calph(ph14,-90) & calph(ph17,-90), caldel(d10,+in10))
  F1PH(calph(ph5,+90)  & calph(ph7,+90) & calph(ph3,-90), caldel(d0,+in0))

HaltAcqu, 1m  ;jump address for protection files
exit                                      ;quit

ph0  = 0
ph1  = 1
ph2  = 0
ph3  = 0 2
ph4  = 1
ph5  = 1 3
ph7  = 0
ph8  = 0
ph9  = 0
ph10 = 0 1 ; phase cycled to eliminate the untransferred CO axial signal
ph11 = 0
ph12 = 0 0 2 2 2 2 0 0
ph14 = 1
ph15 = 0 0 2 2
ph16 = 0
ph17 = 3
ph18 = 0
ph19 = 1
ph20 = 1
ph21 = 1
ph22 = 1
ph23 = 1
ph24 = 1
ph25 = 0
ph26 = 1
ph27 = 2
ph28 = 3
ph29 = 1
ph30 = 0
ph31 = 1 3 3 1 3 1 1 3
```

Listing 8. Bruker pulse program for SIM-(H)N(CA)(CO)NH,(H)CA(N)(CO)CAHA (8-in-1)

```
;sequence for simultaneous acquisition of 8 different 3D spectra
;Avance II+ version
;parameters:
;p1 : 1H 90 pulse @ plw1
;pl1 : 1H power for 90 pulse

;p15 : contact time for H->N CP
;pl2 : 15N power for H->N CP
;sp0 : 1H power for H->N CP
;spnam0 : Ramp90.100
;spoffs0 : 0
;sp18 : Co selective pi
;sp19 : Ca selective pi
;sp24 : Co->N CP
;sp26 : Co->N CP
;sp25 : N->Ca CP
;sp27 : N->Ca CP
;p17 : contact time for N->H CP
;sp1 : H-CalphCP
;pl20 : 15N power for N->H CP
;sp10 : 1H power for N->H CP
;sp29 : 1H to 13Calpha CP
;spnam10 : Ramp100.90
;spoffs10 : 0

;p26 : N -> Co CP
;p27 : Ca -> N CP
;p18 : Co selective pi
;p19 : Ca selective pi
;p7 : 15N 90 pulse @ plw7
;pl7 : 15N power for 90 pulse

;p3 : 13C 90 pulse @ plw3
;pl11 : 13C power for 90 pulse

;cpdprg1 : 1H decoupling (sltppm_40pTr41 for 1Hprot, waltz16_pl12 for 2Hprot)
;cpdprg4 : Water suppression with sltppm or cw_pl18 @ 15kHz
;cpdprg2 : 15N decoupling (waltz16_pl16)
;cpdprg3 : 13C decoupling (waltz16_pl17)

;pl12 : 1H decoupling power for (waltz16)
;pl18 : 1H decoupling for (cw_pl18)
;pl13: 1H decoupling (sltppm)
;p15: combined H-C and H-N forward CP
;pl16: 15N decoupling power (waltz16)
;pl17: 13C decoupling power (waltz16)

;pcpd1 : 25u (waltz16 10 kHz) - 33.33 (sltppm 15kHz)
;pcpd4 : 33.33 (sltppm 15kHz)
;pcpd2 : 25u (waltz16 10 kHz)
;pcpd3 : 25u (waltz16 10 kHz)
;l1 : 1 (both HA and HN), 0 (only HA), 2 (only HN) signal recorded

;$COMMENT=basic cp experiment, arbitrary contact and decoupling schemes
;$CLASS=Solids
;$DIM=1D
;$TYPE=cross polarisation
;$SUBTYPE=simple 1D
;$OWNER=Bruker
prosol relations=<solids_cp>

#include <Avancesolids.incl>

; 1H settings
"spoff6=0.0"
"spoal6=0.5"
"spoff7=0.0"
"spoal7=0.5"

; 15N settings
"plw2=plw7"
```

```
"plw16=plw2*(pow(p7/25,2))"     ; 15N waltz 10kHz decoupling power level
"spoffs2=0"
"spoal2=0.5"
"spoff10=0"
"spoal10=0.5"
"spoal3=0.5"
"spoffs3=0"
"spoal4=0.5"
"spoffs4=0"
"spoal5=0.5"
"spoff5=0"

; 13C settings
"plw11=plw3"
"plw17=plw3*(pow(p3/12.5,2))"     ; 13C DIPSI-3 20kHz decoupling power level

"cnst22 = (sfo3-bf3)*1000000/bf3"  ; CA frequency offset (ppm)
"cnst19 = cnst22+(173.3-53.3)"     ; CO frequency offset (ppm)
"cnst20 = cnst22-(53.3-22.3)"     ; special CB frequency offset (ppm)
"cnst23 = cnst22-(53.3-113.3)"    ; offset in between of CO/CA

"cnst25=360*(cnst22-cnst23)*bf3/2" ; phase change for CA

;"spoff8=0"          ; on-resonance CO, NO: NOW IT IS RELEASED TO ALLOW OFF-RESONANCE CP
;"spoffs8=60*bf3"    ; this can be fixed as a typical solution
              ; BUT IN THIS CASE, PHASE 25 HAS TO BE CORRECTED EMPIRICALLY (PHCOR25 != 0)
"spoal8=0"
"spoff8=bf3*((60+cnst19-cnst23)/1000000)" ; CO offset CA/CO+60ppm

;"spoff9=0"
  ; on-resonance CO, NO: NOW IT IS RELEASED TO ALLOW OFF-RESONANCE CP
;"spoffs9=-60*bf3"   ; this can be fixed as a typical solution
                     ; BUT IN THIS CASE, PHASE 16 HAS TO BE CORRECTED EMPIRICALLY (PHCOR16 != 0)
"spoal9=1"
"spoffs9=bf3*((cnst22-cnst23-60))/1000000" ; CA offset CA/CO-60ppm


"p18=3.412/(95.0*bf3/1000000)"    ; 95 ppm bandwidth (safe)
"spw18=plw3*pow((0.5/(p18*0.1515))/(0.25/p3),2)" ;  Q3 power level
"spoal18=0.5"                      ; default value (irrelevant)
"spoff18=bf3*((cnst19-cnst23)/1000000)" ; CO offset CA/CO

"p19=3.412/(105.0*bf3/1000000)"     ; 105 ppm bandwidth (safe)
"spw19=plw3*pow((0.5/(p19*0.1515))/(0.25/p3),2)" ;  Q3 power level
"spoal19=0.5"                      ; default value (irrelevant)
"spoff19=bf3*((cnst22-cnst23))/1000000" ; CA offset CA/CO

;"p20=4.64/(36*bf3/1000000)"         ; 36 ppm bandwidth for CA  (safe)
;"spw20=plw3*pow((0.5/(p20*0.0798))/(0.25/p3),2)" ;  ReBURP power level
;"spoal20=0.5"                      ; default value (irrelevant)
;"spoff20=0"                         ; CA offset CA

"p25=4.64/(24*bf3/1000000)" ; CB: 24 ppm bandwidth (25+12=37 ppm band; no effect from 25+18=43
  ppm)
"spw25=plw3*pow((0.5/(p25*0.0798))/(0.25/p3),2)" ;  ReBURP power level
"spoal25=0.5"                      ; default value (irrelevant)
"spoff25=bf3*((cnst20-cnst23)/1000000)" ; CB offset from CA/CO

"spoal29=1.0"
"spoff29=0"   ; on-resonance CA
"spoal30=0.0"
"spoff30=0"                                    ; on-resonance CA

"d11=0.5*atan(cnst11*PI*55.0)/(PI*55)"       ; J(CO-CA)=55, relax. CO optimised delay
;d11 : optimised time for J-transfer CO-CA
;cnst11 : approximate T2' (CO)
"d12=0.5*atan(cnst10*PI*55.0)/(PI*55)"   ; J(CO-CA)=55, relax. CA optimised delay
;d12 : optimised time for J-transfer CA-CO
;cnst10 : approximate T2' (CO)

"d9=d12-p25"

"d0=0"
```

```
;d0 : 13CA evolution time in t1
"d15=d0*cnst21"
;d15 : 15N evolution time in t1
;cnst21 : tmax(15N)/tmax(13C) usually 2.4803 (=gamma_C/gamma_N, gives the same ppm step)
"in0=inf1"
;in0 : Time increment for 13CA in t1
"in15=in0*cnst21"
;in15 : Time increment for 15N in t1 (for information only)

"d10=0"
;d10 : 13CA evolution time in t2
"d19=cnst21*d10*2"
;d19 : 15N evolution time in t2
"in10=inf2/2"
;in10 : Time increment for in t2
;d6 : Compensation time for 15N 90 pulse duration
"d6=p7"

;d3 : Compensation time in the 1H echo before acquisition
"d3=trunc((p1+de)*cnst31/1000000+0.9999)*(1s/cnst31)-p1/1000000"
;cnst31 : Rotation frequency [Hz]
;d4 : Compensation time in the 1H echo before acquisition
"d4=d3-de"

;d1 : Inter-scan delay
;d30 : Time for MISSISSIPPI water suppression
"d18=d12-p25"
"d5=0.25/55"
"d2=d5-p25"
"d7=p3/3.14*2"

"d14=larger(0,d18-d10)"
"d13=larger(d10,d10*0.5+d18*0.5)"
"d16=-larger(-d13,-d2)"
"d17=larger(0,d10-d2)"

"cnst26=cnst25*d0"                          ; phase shift CA in t1 (TPPI)
"cnst27=cnst25*d10*2"                       ; phase shift CA in t2 (TPPI)

aqseq 321

if "nbl!=2"
{
  print "Please reserve space for separate FIDs with NBL=2"
}

1 ze

2 d1 do:f2 do:f3
#include <p15_prot.incl>
#include <aq_prot.incl>

  ; 15N evolution periods
  "d15=d0*cnst21"
  "d19=d10*cnst21*2"

   "d14=larger(0,d18-d10)"
   "d13=larger(d10,d10*0.5+d18*0.5)"
   "d16=-larger(-d13,-d2)"
   "d17=larger(0,d10-d2)"

  "cnst26=cnst25*d0"                          ; phase shift CA in t1 (TPPI)
  "cnst27=cnst25*d10*2"                            ; phase shift CA in t2 (TPPI)

  10u ip24+cnst26
  10u ip21+cnst27

  1m st0

#ifndef NOSEPARATION
  if (l2 != 1) {
       print "error: Mixing l2 separation of +/- components and F2I extra loop may lead to confus-
  ing (unintended) results"
```

```
      goto HaltAcqu
  }
#endif

1u fq=cnst22 (bf ppm):f3               ; offset CA

(p1 pl1 ph1):f1
(p29:sp29 ph1 p3 pl11 ph0 10u fq=cnst23(bf ppm)):f3 (p15:sp4 ph2):f2 (p15:sp6 ph0):f1
(1u cpds1):f1

; 15N co-evolution in t1 (while 13CA is flipped back to z)
if (l3 == 0) {
       if "d15 >= p3*4" {
              (center (d15) (p3 ph0 p3*2 ph1 p3 ph0):f3)
              (p7 pl7 ph0):f2                              ; flip-up 15N
       } else {
              d15
              (p7 pl7 ph0):f2 (p3 ph0 p3*2 ph1 p3 ph0):f3
                                          ; flip-up 15N and perform the missing 13C pulses
       }
  } else {                                ; do not perform any inversion pulses to save S/N
       d15
       (p7 pl7 ph0):f2                              ; flip-up 15N
  }

  1m                                          ; z-filter

  ; 13CA and frequency encoding
  (p3 pl11 ph16:r):f3                                                  ; flip-down 13CA
  d0*0.5
  2u
  if (l3 == 0) {
       (center (p18:sp18 ph0):f3 (p7 ph0 pl7 p7*2 ph1 pl7 p7 ph0 pl7):f2)
                                          ; CO and 15N J-refocusing pulses
  } else {
       (p18:sp18 ph0):f3                  ; no 15N inversion pulses
  }
  d0*0.5
  d6                  ; compensation delay for 15N 90 pulse
  (p19:sp19 ph24):f3  ; CA non-selective pulse
  1u
  d7
  (p18:sp18 ph0):f3   ; CO BS pulse
  1u

  (p7 pl7 ph0):f2 (1u do):f1;    ;flip N back to xy for CP

  ;;;;;;;;;;;;;;;;;;;;;;;;
  ;;;;;;;  CA-N CP  ;;;;;;
  ;;;;;;;;;;;;;;;;;;;;;;;;

  if (l4 == 1) {
       (p27:sp9 ph1):f3 (p27:sp3 ph1):f2
  } else {
       (p27:sp9 ph1):f3 (p27:sp3 ph5):f2
                  ; steer with extra phases to check whether the pathway goes through this CP
  }
  if (l2 == 0) {
       (1u cpds1):f1   ; switch off this pathway by not executing the flip-up pulse
  } else {
       (p7 pl7 ph18):f2 (1u cpds1):f1   ; flip-up 15N
  }

;;;; Ca-CO transfer
  1u
  (p18:sp18 ph0):f3                ;CO selective Pi
  d7
  d9*0.5
  (p25:sp25 ph0):f3
  d9*0.5
  if (l2 != 2) {      ; if l2 == 2, switch off this pathway by not executing the 180 pulse
       (p19:sp19 ph0):f3 ; CA(B)
```

```
  }
  1u
  (p18:sp18 ph0):f3  ;CO selective Pi
  d9*0.5
  (p25:sp25 ph0):f3
  d9*0.5
  d6                  ; compensation delay for 15N 90 pulse

  (p3 pl11 ph1):f3    ; deexcite CA and excite CO
  d6
  d11
  (p19:sp19 ph0):f3    ; CA selective pi
  1u
  if (l2 != 2) {             ; if l2 == 2, switch off this pathway by not executing the 180 pulse
    (p18:sp18 ph1):f3        ;CO selective Pi
  }
  1u
  d11
  (p19:sp19 ph0):f3    ; CA selective pi
;;;;end of Ca-CO transfer

  d7
  if (l2 == 0) {
       (center (d6)(1u do):f1)     ; switch off this pathway by not executing the flip-down pulse
  } else {
       (p7 pl7 ph0):f2 (1u do):f1  ; flip-down stored 15N magnetisation
  }
  ;;;;;;;;;;;;;;;;;;;;;;;;
  ;;;;;;;  CO-N CP  ;;;;;;
  ;;;;;;;;;;;;;;;;;;;;;;;;
  if (l4 == 1) {
       (p26:sp8 ph1):f3 (p26:sp2 ph1):f2
  } else {
       (p26:sp8 ph8):f3 (p26:sp2 ph1):f2
                      ; steer with extra phases to check whether the pathway goes through this CP
  }
  ;;;;;;;;;;;;;;;;;;;;;;;;
  ;;;;;;;;;;;;;;;;;;;;;;;;
  if (l3 == 0) {
       (p7 pl7 ph20):f2 (1u cpds1):f1 ; flip-up (store) 15N (different by 180 deg)
  } else {
       (p7 pl7 ph0):f2 (1u cpds1):f1 ; flip-up (store) 15N
  }

  ; transfer CO to CA
  1u
  d7
  (p19:sp19 ph0):f3    ; CA selective pi
  d11
  1u
  (p18:sp18 ph17:r):f3       ; CO selective Pi
  2u
  (p19:sp19 ph0):f3          ; CA selective pi
  d11
  d6

  (p3 pl11 ph1):f3 ; deexcite CA and excite CO

  d14*0.5
  if (l3 == 0) {
       (center (p25:sp25 ph0):f3 (p7 pl7 ph0 p7*2 pl7 ph1 p7 pl7 ph0):f2)
  } else {
       (p25:sp25 ph0):f3 ; CB pulse
  }
  d14*0.5
  (p18:sp18 ph0):f3 ; CO selective Pi
  4u
  (p19:sp19 ph21):f3 ; CA/CB selective Pi
  d13
  if (l3 == 0) {
       (center (p25:sp25 ph0):f3 (p7 pl7 ph0 p7*2 pl7 ph1 p7 pl7 ph0):f2)
  } else {
       (p25:sp25 ph0):f3 ; CB pulse
```

```
  }
  d16
  (p18:sp18 ph0):f3 ; CO selective Pi
  d17
  4u
  (p3 pl11 ph15):f3    ;C 90 (flip-up)
  1u

  1m                                          ; z-filter

  ; 15N co-evolution in t2
  if (l3 == 0) {
       if "d19 >= p3*4" {
              (p7 pl7 ph0):f2    ; flip-down 15N
              (center (d19) (p3 ph0 p3*2 ph1 p3 ph0):f3)
       } else {
         (p3 ph0 p3*2 ph1 p3 ph0):f3
         (p7 pl7 ph0):f2    ; flip-down 15N
         d19
       }
  } else {          ; do not perform any inversion pulses to save S/N
              (p7 pl7 ph0):f2                                  ; flip-down 15N
              d19
  }
  (p7 pl7 ph10):f2  (1u do):f1      ; flip-up 15N for water suppression period

;;;;;;;;;;;;;;;; water suppression block starts
  1u pl12:f1
  (d30*0.25 cw ph0 ):f1
  (d30*0.25 cw ph1):f1
  (d30*0.25 cw ph20):f1
  (d30*0.25 cw ph30):f1
  1u do:f1
;;;;;;;;;;;;;;;; water suppression block ends

if (l1 != 2)
{                                          ; collect 13CA->1HA signal
  10u fq=cnst22 (bf ppm):f3                ; offset CA
  (p3  pl11 ph0):f3
  (p30:sp30 ph1):f3 (p30:sp7 ph0):f1
  d3
  (p1*2 pl1 ph0):f1
  d4
}
if (l1 == 0) {
  if (l4 == 1) {
       go=2   ph31 cpds3:f3 finally do:f3
  }
  if (l4 == 2) {
       go=2   ph27 cpds3:f3 finally do:f3
  }
  if (l4 == 3) {
       go=2   ph28 cpds3:f3 finally do:f3
  }
  if (l4 == 4) {
       go=2   ph29 cpds3:f3 finally do:f3
  }
  if (l4 == 5) {
       go=2   ph31 cpds3:f3 finally do:f3
  }
}
if (l1 == 1) {
  if (l4 == 1) {
       goscnp   ph31 cpds3:f3 finally do:f3
  }
  if (l4 == 2) {
       goscnp   ph27 cpds3:f3 finally do:f3
  }
  if (l4 == 3) {
       goscnp   ph28 cpds3:f3 finally do:f3
  }
  if (l4 == 4) {
       goscnp   ph29 cpds3:f3 finally do:f3
```

```
  }
  if (l4 == 5) {
       goscnp   ph31 cpds3:f3 finally do:f3
  }
}

1m st         ; store HN and HA in the independent FIDs (change a memory buffer)

if (l1 != 0)
{
  (p7 pl7  ph0):f2
  (p17:sp5 ph1):f2 (p17:sp10 ph0):f1
  d3
  (p1*2 pl1 ph0):f1
  d4

  if (l4 == 1) {
       go=2   ph31 cpds2:f2 finally do:f2
  }
  if (l4 == 2) {
       go=2   ph27 cpds2:f2 finally do:f2
  }
  if (l4 == 3) {
       go=2   ph28 cpds2:f2 finally do:f2
  }
  if (l4 == 4) {
       go=2   ph29 cpds2:f2 finally do:f2
  }
  if (l4 == 5) {
       go=2   ph31 cpds2:f2 finally do:f2
  }
}

  10m mc #0 to 2
  F1PH(calph(ph2, +90) & calph(ph16, +90), caldel(d0, +in0) & calph(ph2,+90) & calph(ph16,+90))
#ifndef NOSEPARATION
  F2I(ip18*2, 2) ; intended to be the innermost loop
#endif
  F2PH(calph(ph10, -90) & calph(ph15, -90), caldel(d10, +in10))
  F3QF()  ; a fake loop just to allow st commands, always td3=2 (but automatically divided by NBL)

HaltAcqu, 1m  ;jump address for protection files
exit                                        ;quit
ph0 = 0                      ; phase = 0 (constant, multiple uses)
ph1 = 1                      ; phase = 1 (constant, multiple uses)
ph2 = 1 3                    ; 15N phase in H-X CP
ph5 = {1}*4 {3}*4            ; 15N  phase in CA-N CP (used if l4 != 1)
ph8 = {1}*8 {3}*8            ; 13CO phase in CO-N CP (used if l4 != 1)
ph10 = 0 0 2 2               ; 15N flip-up pulse after 2nd evolution
ph15 = 0 0 2 2               ; 90 CA de-exciting pulse after the second evolution
ph16 = 0 2                   ; 90 pulse before 13CA t1 evolution
ph17 = 1                     ; CO-selective 180 pulse in the second CO-CA J-transfer
ph18 = 0                     ; 15N 90 just after CA-N CP
ph20 = 2                     ; phase = 2 (constant)
ph21 = 0                     ; 13CA refoc pulse in t2 (CA)
ph24 = 0                     ; 13CA refoc pulse in t1 (CA)
ph27 = {{1 3 3 1}^2}^2 ; alternative receiver (16 scans min) to observe class   I pathways (l4=2)
ph28 = {{1 3 3 1}^2}*2 ; alternative receiver (16 scans min) to observe class  II pathways (l4=3)
ph29 = {{1 3 3 1}*2}^2 ; alternative receiver (16 scans min) to observe class III pathways (l4=4)
ph30 = 3                     ; phase = 3 (constant)
ph31 = 1 3 3 1               ; RECEIVER to observe class IV pathways (l4=5) or all pathways
```

K. References

(1) Gopinath, T.; Veglia, G. Dual acquisition magic-angle spinning solid-state NMR-spectroscopy: simultaneous acquisition of multidimensional spectra of biomacromolecules*; Angew. Chem. Int. Ed. Engl.* **2012**, *51*, 2731-2735.

(2) Bak, M.; Rasmussen, J. T.; Nielsen, N. C. SIMPSON: a general simulation program for solid-state NMR spectroscopy*; J. Magn. Reson.* **2000**, *147*, 296-330.

(3) Emsley, L.; Bodenhausen, G. Optimization of Shaped Selective Pulses for NMR Using a Quaternion Description of Their Overall Propagators*; J. Magn. Reson.* **1992**, *97*, 135-148.

(4) Geen, H.; Freeman, R. Band-Selective Radiofrequency Pulses*; J. Magn. Reson.* **1991**, *93*, 93-141.

(5) Bennett, A. E.; Rienstra, C. M.; Auger, M.; Lakshmi, K. V.; Griffin, R. G. Heteronuclear decoupling in rotating solids*; J. Chem. Phys.* **1995**, *103*, 6951-6958.

(6) Lewandowski, J. R.; Sein, J.; Sass, H. J.; Grzesiek, S.; Blackledge, M.; Emsley, L. Measurement of site-specific 13C spin-lattice relaxation in a crystalline protein*; J. Am. Chem. Soc.* **2010**, *132*, 8252-8254.

(7) Shaka, A. J.; Keeler, J.; Frenkiel, T.; Freeman, R. An Improved Sequence for Broad-Band Decoupling - WALTZ-16*; J. Magn. Reson.* **1983**, *52*, 335-338.

(8) Shaka, A. J.; Lee, C. J.; Pines, A. Iterative schemes for bilinear operators; application to spin decoupling*; J. Magn. Reson. (1969)* **1988**, *77*, 274-293.

(9) Zhou, D. H.; Rienstra, C. M. High-performance solvent suppression for proton detected solid-state NMR*; J. Magn. Reson.* **2008**, *192*, 167-172.

(10) States, D. J.; Haberkorn, R. A.; Ruben, D. J. A Two-Dimensional Nuclear Overhauser Experiment with Pure Absorption Phase in 4 Quadrants*; J. Magn. Reson.* **1982**, *48*, 286-292.

(11) Hediger, S.; Meier, B. H.; Kurur, N. D.; Bodenhausen, G.; Ernst, R. R. NMR cross polarization by adiabatic passage through the Hartmann—Hahn condition (APHH)*; Chem. Phys. Lett.* **1994**, *223*, 283-288.

(12) Evenas, J.; Tugarinov, V.; Skrynnikov, N. R.; Goto, N. K.; Muhandiram, R.; Kay, L. E. Ligand-induced structural changes to maltodextrin-binding protein as studied by solution NMR spectroscopy*; J. Mol. Biol.* **2001**, *309*, 961-974.

(13) Venters, R. A.; Farmer, B. T., 2nd; Fierke, C. A.; Spicer, L. D. Characterizing the use of perdeuteration in NMR studies of large proteins: 13C, 15N and 1H assignments of human carbonic anhydrase II*; J. Mol. Biol.* **1996**, *264*, 1101-1116.

(14) Zhou, D. H.; Shah, G.; Cormos, M.; Mullen, C.; Sandoz, D.; Rienstra, C. M. Proton-detected solid-state NMR spectroscopy of fully protonated proteins at 40 kHz magic-angle spinning*; J. Am. Chem. Soc.* **2007**, *129*, 11791-11801.